# A transient protein folding response targets aggregation in the early phase of TDP-43-mediated disease

Rebecca San Gil[1], Dana Pascovici[2,3], Juliana Venturato[1], Heledd Brown-Wright[1], Prachi Mehta[1,4], Lidia Madrid San Martin[1], Jemma Wu[3], Wei Luan[1], Yi Kit Chui[1], Adekunle T. Bademosi[1], Shilpa Swaminathan[1], Serey Naidoo[5,6], Britt A. Berning[1], Amanda L. Wright[1], Sean S. Keating[1], Maurice A. Curtis[6,7], Richard L. M. Faull[6,7], John D. Lee[8], Shyuan T. Ngo[9], Albert Lee[4], Marco Morsch[4], Roger S. Chung[4], Emma Scotter[5,6], Leszek Lisowski[10,11,12], Mehdi Mirzaei[3], Adam K. Walker[1*]

[1] Neurodegeneration Pathobiology Laboratory, Clem Jones Centre for Ageing Dementia Research, Queensland Brain Institute, The University of Queensland, Brisbane, QLD, Australia

[2] Insight Stats, Croydon Park, NSW, Australia

[3] Macquarie Medical School, Faculty of Medicine, Health and Human Sciences, Macquarie University, North Ryde Sydney, New South Wales, Australia

[4] Motor Neuron Disease Research Centre, Macquarie Medical School, Macquarie University, Sydney, NSW, Australia

[5] School of Biological Sciences, University of Auckland, Auckland, New Zealand

[6] Centre for Brain Research, University of Auckland, Auckland, New Zealand

[7] Department of Anatomy and Medical Imaging, University of Auckland, Auckland, New Zealand

[8] School of Biomedical Sciences, Faculty of Medicine, The University of Queensland, St Lucia, Brisbane, QLD, Australia

[9] Australian Institute for Bioengineering and Nanotechnology, The University of Queensland, Brisbane, Queensland, Australia

[10] Vector and Genome Engineering Facility, Children's Medical Research Institute, Westmead, New South Wales, Australia

[11] Laboratory of Molecular Oncology and Innovative Therapies, Military Institute of Medicine – National Research Institute, Warsaw, Poland

[12] Translational Vectorology Research Unit, Children's Medical Research Institute, Faculty of Medicine and Health, The University of Sydney, Westmead, Australia

* Corresponding author Adam K. Walker, email: adam.walker@uq.edu.au

## SUPPLEMENTARY INFORMATION

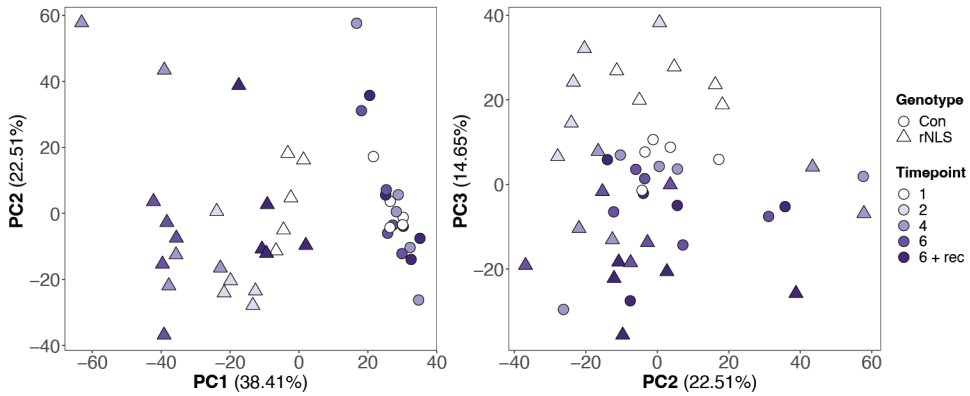


**Supplementary Figure 1. Principal component analysis (PCA).** *Left:* PC1 resolves samples by mouse genotype versus PC2. *Right* : PC2 versus PC3 resolves samples by timepoint (proportion of variation from top 5 PC in parentheses). The proteins with the highest PCA loadings for PC1 include serine/threonine-protein kinase DCLK1, protein kinase C beta type, and protein phosphatase 3 catalytic subunit alpha. Proteins with the highest PCA loadings for PC2 include 116 kDa U5 small nuclear ribonucleoprotein component, ras-related protein Rab-12, and secretory carrier-associated membrane protein 5. Proteins with the highest PCA loadings for PC3 include heat shock protein HSP 90-beta, small ribosomal subunit protein uS15m, and voltage-gated potassium channel subunit beta-2. Source data are provided as a Source Data file.

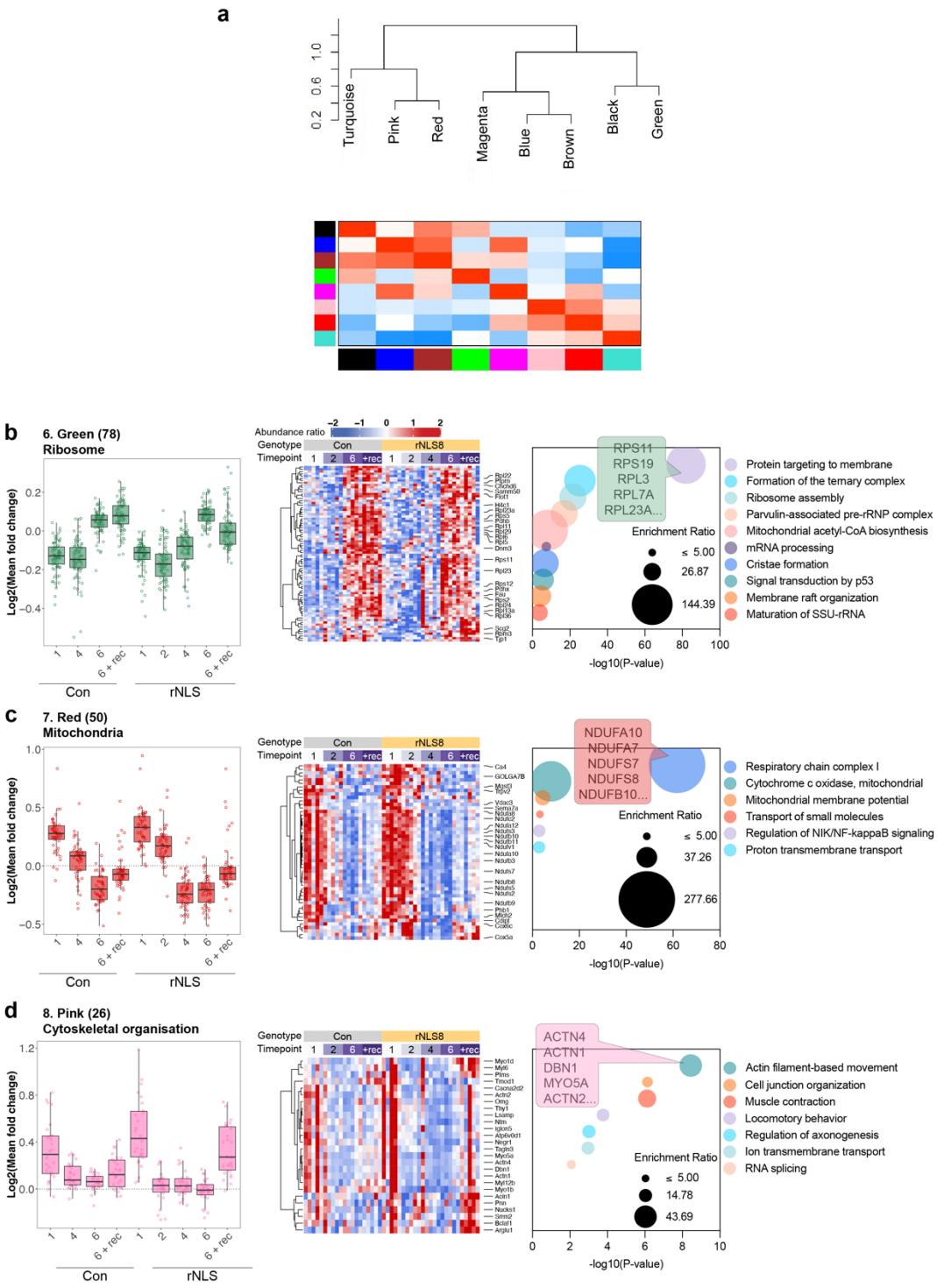


**Supplementary Figure 2. Weighted correlation network analysis reveals 8 defined modules in proteomics of control and rNLS8 mice, of which three are age dependent. a,** Module eigenprotein network showing hierarchical clustering and heatmap of eigenprotein correlation adjacency table. Red in the heatmap represents more closely correlated modules. **b-c,** green, red, and pink modules are age-dependent modules that show similar changes in protein abundance in control and rNLS8 mice, which may be attributed to the age of the mice at the timepoints analyzed. The number of proteins in each module is listed in parentheses. *Left,* Log fold change of module proteins in control and rNLS8 samples at each disease stage. *Center*, Heat map of module proteins. *Right,* Gene ontology of the biological processes enriched in each module. The size of the circles is dependent on enrichment ratio and the top 5 proteins belonging to the most significant term are shown ranked by kMe value (module membership score) for **b,** green (ribosome), **c,** red (mitochondria), and **d,** pink (cytoskeletal organization) modules. Source data are provided as a Source Data file.

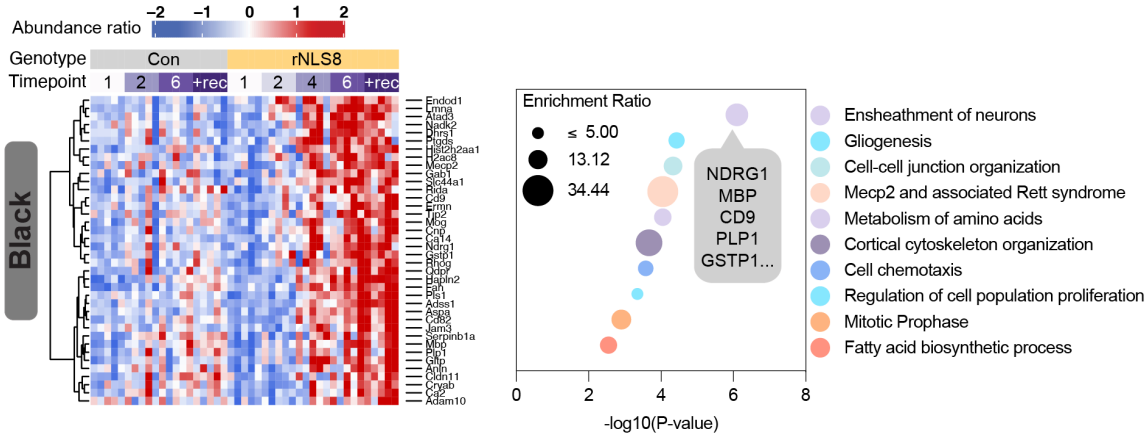


**Supplementary Figure 3. Gene ontology analysis of the black module identifies myelin ensheathment of neurons and gliogenesis as key increased pathways in the rNLS8 cortex.** Proteins in the black module showed a time-dependent increase in abundance in rNLS8 mouse cortex but were stable across time in control animals (Figure 3c). The abundance of these proteins remained high in rNLS8 cortex in recovery, suggesting that disease-associated changes in this module may not directly correlate with TDP-43 pathology burden, and these alterations may be required for initiation of motor recovery after inhibition of hTDP-43$^{\Delta NLS}$ expression. Proteins in the black module were enriched in proteins expressed highly in oligodendrocytes, the myelinating glia of the central nervous system (enrichment ratio = 4.79, $P < 0.00001$; Figure 3g). Complex heatmap of protein abundance ratios (*left*) of each protein identified in the black module and the top 10 gene ontology terms plotted by significance (*right*). Overlaid with callouts that list 5 proteins that comprise the top biological process in each module ranked by kME value. Source data are provided as a Source Data file.

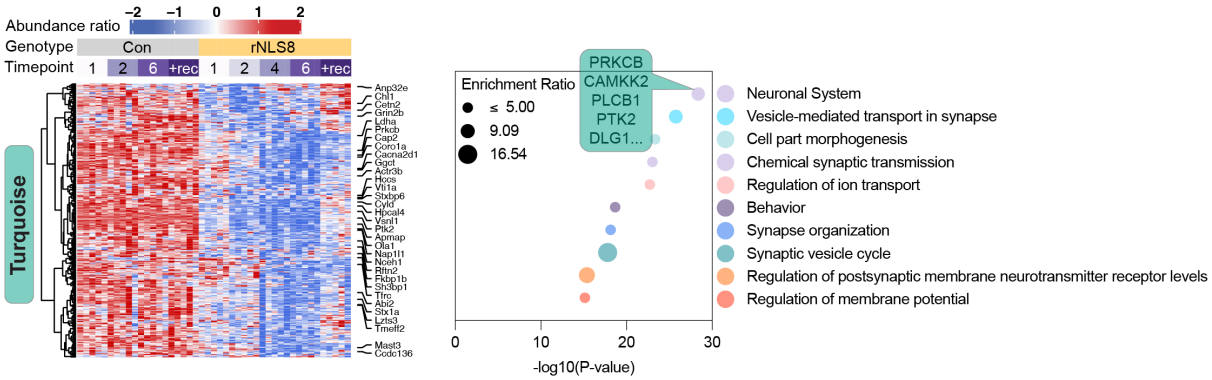


**Supplementary Figure 4. Gene ontology of protein subsets that comprise the turquoise module identifies the neuronal system as a key decreased pathway in disease.** Complex heatmaps of protein abundance ratios (*left*) of each protein identified in the turquoise module and the top 10 gene ontology terms plotted by significance (*right*). Overlaid with callouts that list 5 proteins that comprise the top biological process in each module ranked by kME value. Source data are provided as a Source Data file.

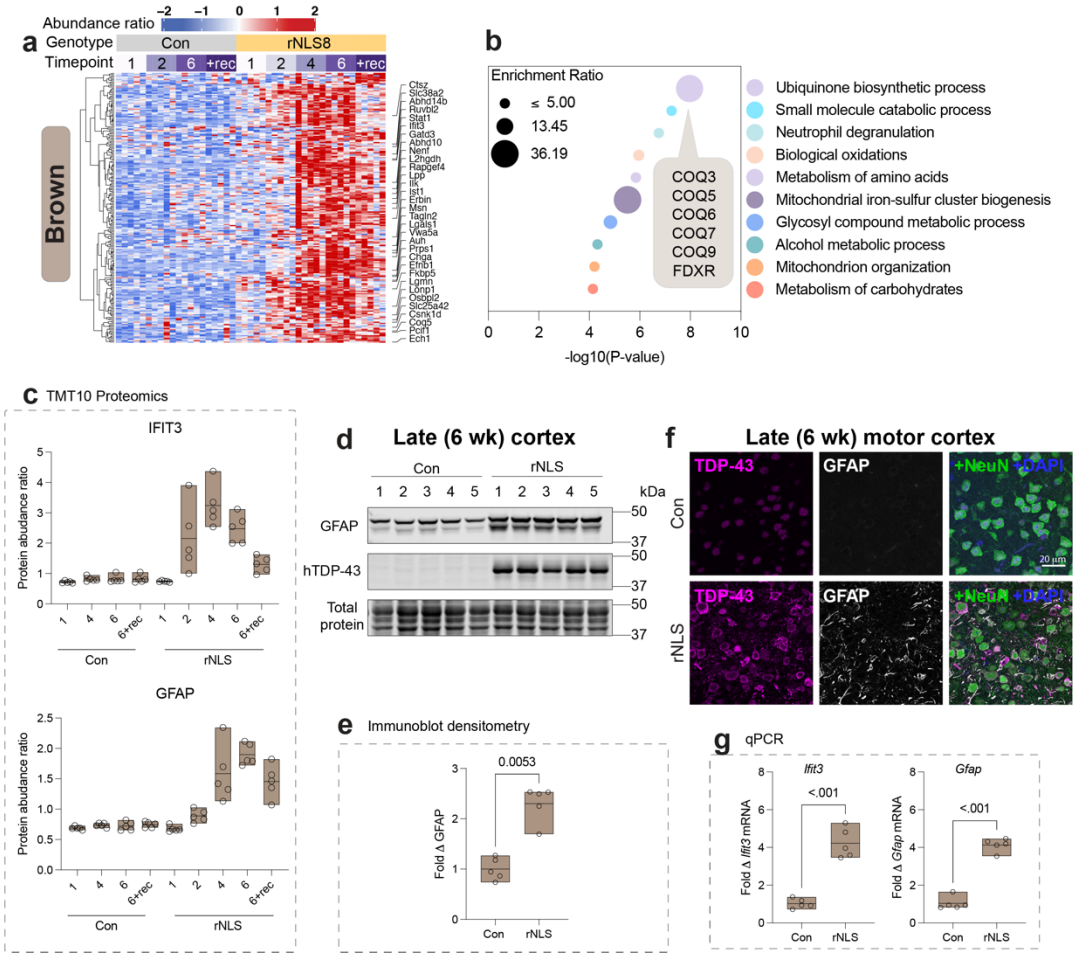


**Supplementary Figure 5. Gene ontology analysis revealed that the brown module was enriched in ubiquinone biosynthesis and small molecule catabolic processes that are increased in late disease and are partially reversed with recovery in rNLS8 mice.** Proteins in the brown module showed a time-dependent increase in abundance in rNLS8 mice beginning in later disease stages, with no change over time in control mice. The elevated abundance of these proteins was partially reversed in rNLS8 recovery mice compared to controls. The brown module was enriched for microglial proteins (enrichment ratio = 2.05, $P < 0.05$) (Figure 3g). **a,** Heatmap of protein abundance of all proteins in the brown (catabolism) module. **b,** Gene ontology of enriched biological processes in the brown module. Ranked by P-value and circle size is dependent on enrichment ratio. **c,** Protein abundance ratio from quantitative temporal proteomics of interferon-induced protein with tetratricopeptide repeats 3 (IFIT3) and glial fibrillary acid protein (GFAP). IFIT3, an antiviral protein expressed in response to interferon-alpha, and GFAP, a marker of astrogliosis, exhibited the highest fold changes in the brown module. **d,** Immunoblot of RIPA-soluble whole cortex tissue lysates after 6 weeks of cytoplasmic TDP-43 expression. Tissue was probed for GFAP (50 kDa) and human TDP-43 (43 kDa). **e,** Immunoblot densitometry, fold change protein levels relative to the mean of control mice and normalized to total protein loading. **f,** Immunofluorescence microscopy of the primary motor cortex in control and rNLS8 mice after 6 weeks of cytoplasmic TDP-43 expression. Samples were immunolabeled for GFAP (*top to bottom*), and co-labeled for TDP-43, NeuN (pan-neuronal marker) and DAPI. Scale bar = 20 μm. **g,** Fold change in mRNA transcript level of target genes relative to the mean of control mice and normalized to GAPDH housekeeping gene by qPCR. Antibodies tested against IFIT3 were ineffective; however, we detected a 4.2-fold increase in *Ifit3* mRNA in cortex tissue from mice in late disease, suggesting that the brown module represents transcriptionally mediated inflammatory activation. GFAP demonstrated an increase in mRNA (4.1-fold increase), protein levels by immunoblot (2.3-fold increase), and astrocytic localization by immunohistochemistry in late-disease cortex tissue. All data is from n = 5 mice per group (open circle points) with a line at the mean and range displayed by floating bars. Differences in the means of control and rNLS8 mice were determined using a two-tailed paired t-test, where a value of $P < 0.05$ was considered statistically significant. Source data are provided as a Source Data file.

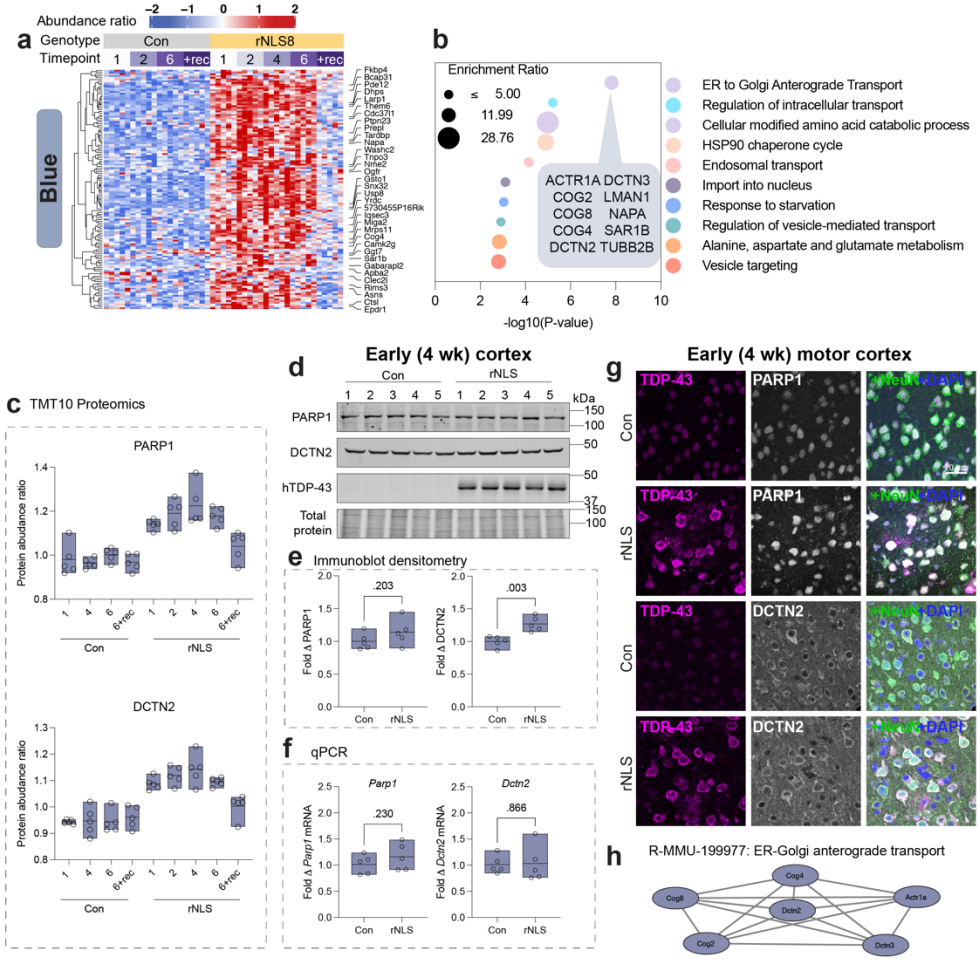


**Supplementary Figure 6. Proteins involved in transport in the blue module demonstrate early and sustained altered levels in the rNLS8 cortex that return to control levels in recovery.** The blue module was characterized by early increases in abundance at pre-onset (1 wk) that were sustained throughout the disease course in the rNLS8 cortex, with no change over time in control mice (Figure 3c). The abundance of proteins in the blue module returned to control levels in recovery and correlated with levels of hTDP-43ΔNLS. **a,** Heatmap of protein abundance of all proteins in the blue module. **b,** Gene ontology of enriched biological processes in the blue module revealed that ER to Golgi anterograde transport and regulation of intracellular transport were the top two significantly enriched biological processes. Ranked by P-value, with circle size being dependent on enrichment ratio. **c,** Protein abundance ratio from quantitative temporal proteomics of Poly [ADP-ribose] polymerase 1 (PARP1) and dynactin subunit 2 (DCTN2). **d,** Immunoblot of RIPA-soluble whole cortex tissue lysates after 4 weeks of cytoplasmic TDP-43 expression. Tissue was probed for PARP1 (115 kDa), DCTN2 (50 kDa), and human TDP-43 (43 kDa). **e,** Immunoblot densitometry, fold change protein levels relative to the mean of control mice and normalized to total protein loading. **f**, Fold change in mRNA transcript level of target genes relative to the mean of control mice and normalized to the GAPDH housekeeping gene by qPCR. Immunoblotting and immunohistochemistry validated the increase in DCTN2 in rNLS8 mice compared to controls; however, there was no change in *Dctn2* transcript level, indicating that protein level increases were not due to increased gene expression. All data are from n = 5 mice per group (open circle points) with a line at the mean and range displayed by floating bars. Differences in the means of control and rNLS8 mice were determined using a two-tailed paired t-test, where a value of $P < 0.05$ was considered statistically significant. **g,** Immunofluorescence microscopy of the primary motor cortex in control and rNLS8 mice in early disease (4 wk). Samples were immunolabeled for each target, PARP1 and DCTN2 (*top to bottom*), and co-labeled for TDP-43, NeuN (pan-neuronal marker) and DAPI. Scale bar = 20 μm. Immunohistochemistry validated the increase in PARP1 in the nucleus of neurons in the primary motor cortex of rNLS8 mice compared to controls, but there was no significant change in *Parp1* at the transcript level or by immunoblot. **h,** Protein-protein interaction network for proteins, including DCTN2, in the blue module that are involved in ER to Golgi anterograde transport. Source data are provided as a Source Data file.

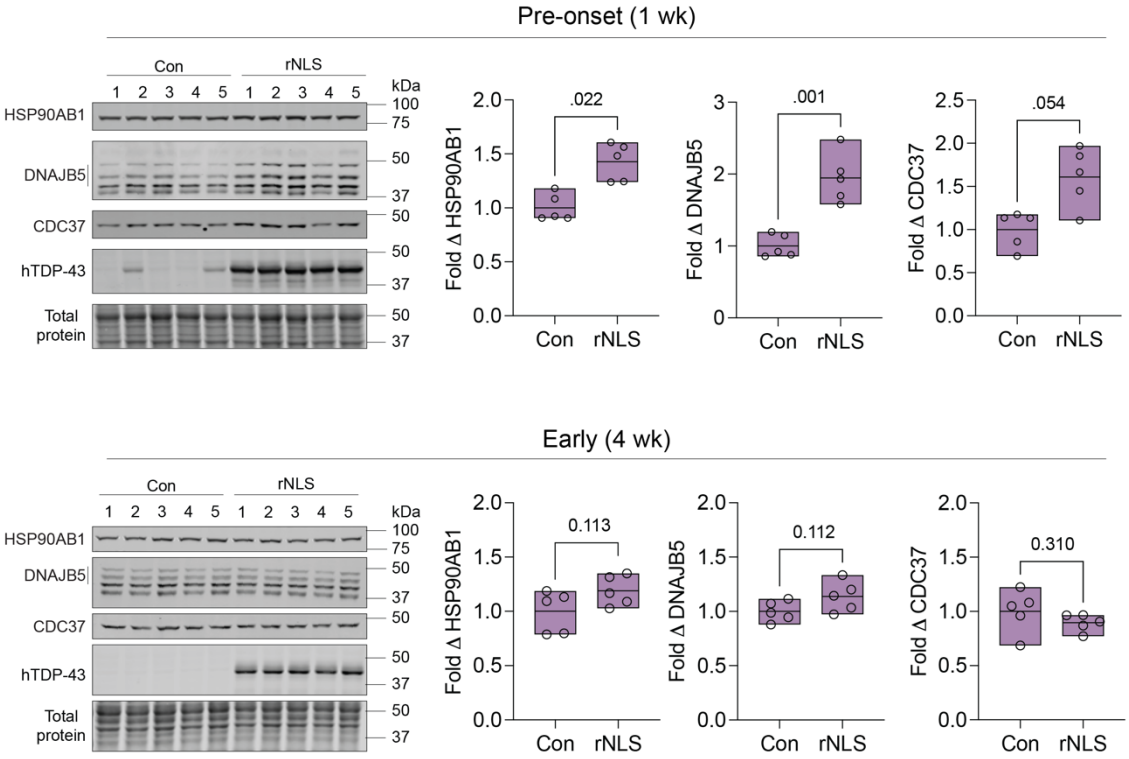


**Supplementary Figure 7. Magenta module proteins, HSP90AB1, DNAJB5 and CDC37 are increased at pre-onset and disease onset but normalize to control levels in early disease.** Immunoblot analysis of control and rNLS8 mouse cortex RIPA-soluble lysates at pre-onset (1 wk; top) and in early disease (4 wk; bottom). Samples were probed for HSP90AB1, DNAJB5, CDC37, TDP-43, and Revert total protein stain and the relative abundance of each protein was normalized to the total protein loading. Data are presented as open circles to represent individual mice (n = 5/group), and floating bars show the mean and range of the data. Differences between the means were determined using a paired t-test, where $P<0.05$ was considered statistically significant. Source data are provided as a Source Data file.

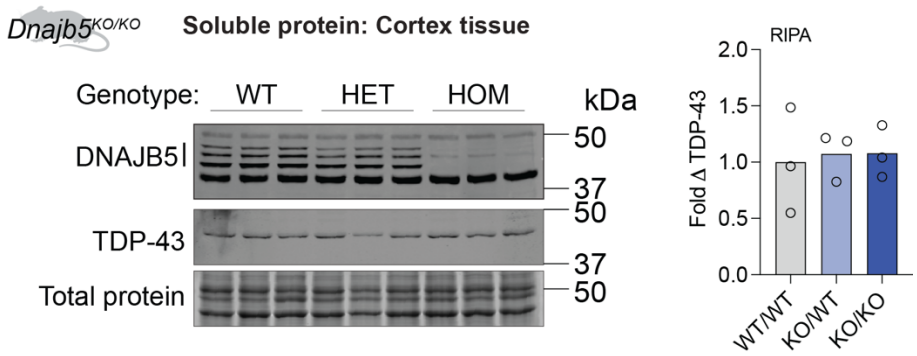


**Supplementary Figure 8. Validation of DNAJB5 antibody in *Dnajb5*$^{KO/KO}$ knockout mice.** RIPA-soluble cortex tissue from wild-type (WT/WT), heterozygous DNAJB5 knockout (KO/WT) and homozygous DNAJB5 knockout (KO/KO) mice (n = 3) were probed for DNAJB5 using the Proteintech 16453-1-AP antibody and TDP-43. The DNAJB5 antibody detected multiple bands between 37-75 kDa, three of which were eliminated or decreased with DNAJB5 KO that represent DNAJB5 isoforms in the cortex. Source data are provided as a Source Data file.

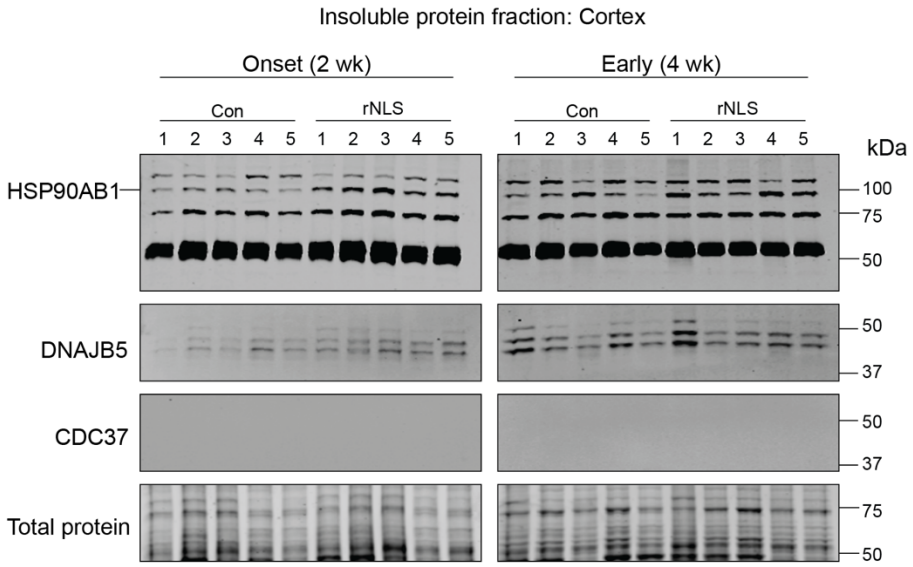


**Supplementary Figure 9. Not all chaperone proteins in the magenta module are sequestered to the insoluble protein fraction in the cortex of rNLS8 mice.** The cortex of rNLS8 mice at onset (2 wk) and in early disease (4 wk) was harvested and fractionated into soluble and insoluble fractions. The insoluble protein fraction was immunoblotted and probed for HSP90AB1, DNAJB5, and CDC37 to determine whether there was sequestration of these proteins into the insoluble fraction. We observed HSP90AB1 and DNAJB5 in the insoluble fraction of control and rNLS8 cortex tissue at disease onset and early disease, but there was no insoluble CDC37 at either timepoint. Data from n = 5 mice per group.

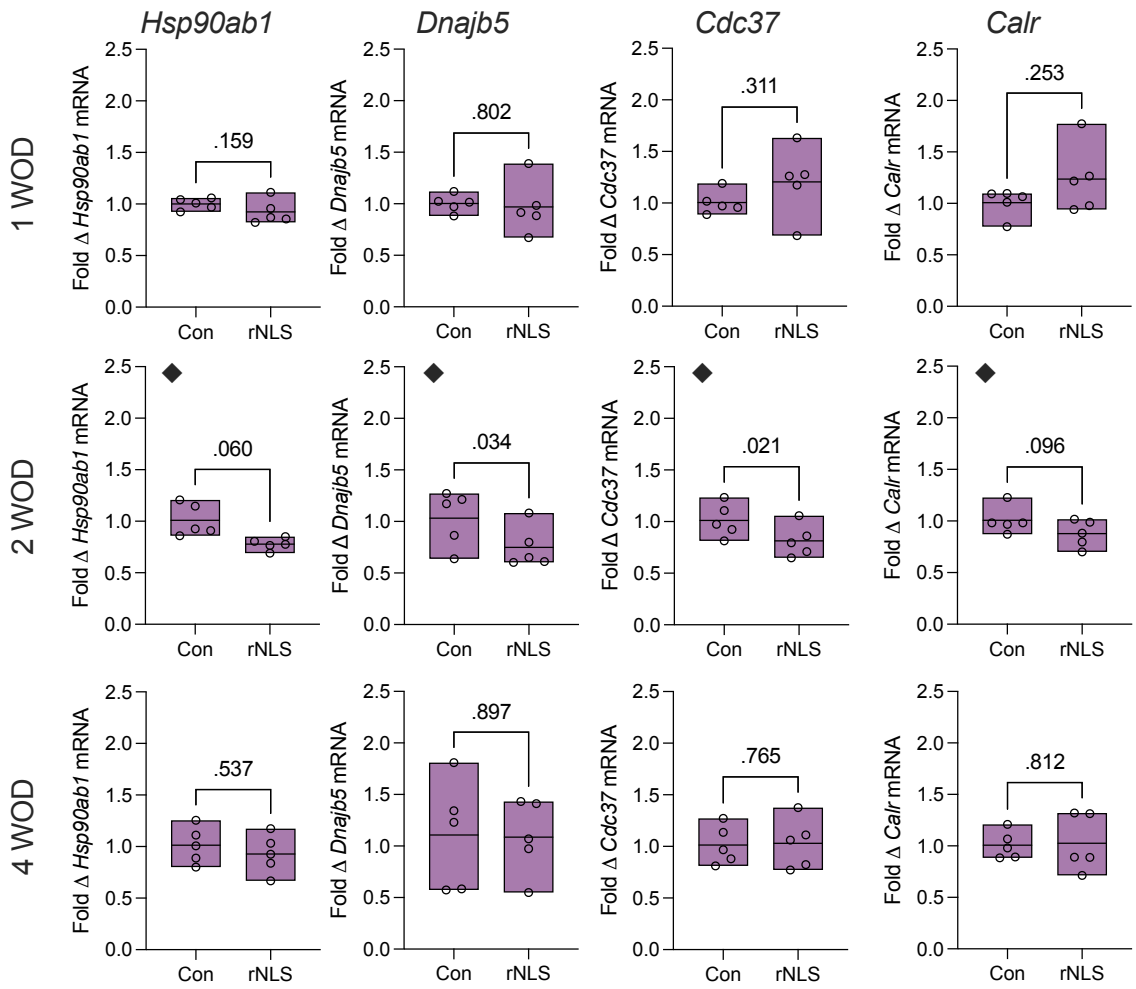


**Supplementary Figure 10. Transcript levels of magenta module proteins are not significantly increased in the cortex of rNLS8 mice, despite increased protein levels at pre-onset and onset shown in Figure 4 and Supplementary Figure 8.** ◆ Denotes data that was shown in Figure 4, which are shown again here for a complete dataset of the transcript levels at each timepoint, pre-onset (1 wk), onset (2 wk) and early disease (4 wk). Data are shown as the fold change in mRNA transcript level of target genes relative to the mean of control mice and normalized to the GAPDH housekeeping gene by qPCR. All data are from n = 5 mice per group (open circle points) with a line at the mean and range displayed by floating bars. Differences in the means of control and rNLS8 mice were determined using a two-tailed paired t-test, where $P < 0.05$ was considered statistically significant. Source data are provided as a Source Data file.

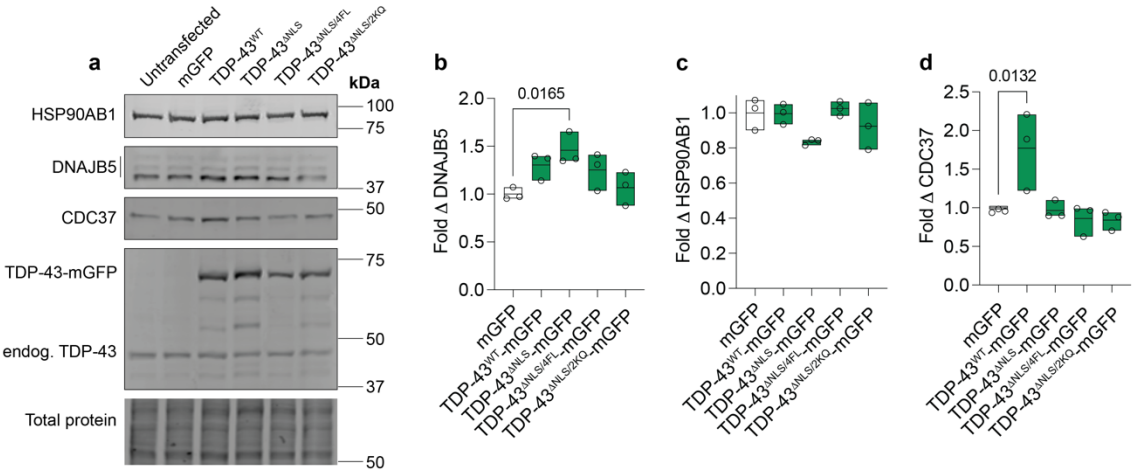


**Supplementary Figure 11. Over-expression of cytoplasmic TDP-43 variants has a variable effect on chaperone abundance in HEK293 cells.** HEK293 cells were transfected to express WT or cytoplasmic mutant TDP-43 for 48 h. **a,** RIPA soluble proteins were immunoblotted and probed for HSP90AB1, DNAJB5, and CDC37. **b,** Fold change DNAJB5. **c**, Fold change HSP90AB1. **d,** Fold change CDC37. All data are from n = 3 independent experiments (open circles) with a line at the mean and the range displayed by floating bars. Differences in the means were determined using a one-way ANOVA and Dunnett's posthoc test, where $P < 0.05$ was considered statistically significant. Source data are provided as a Source Data file.

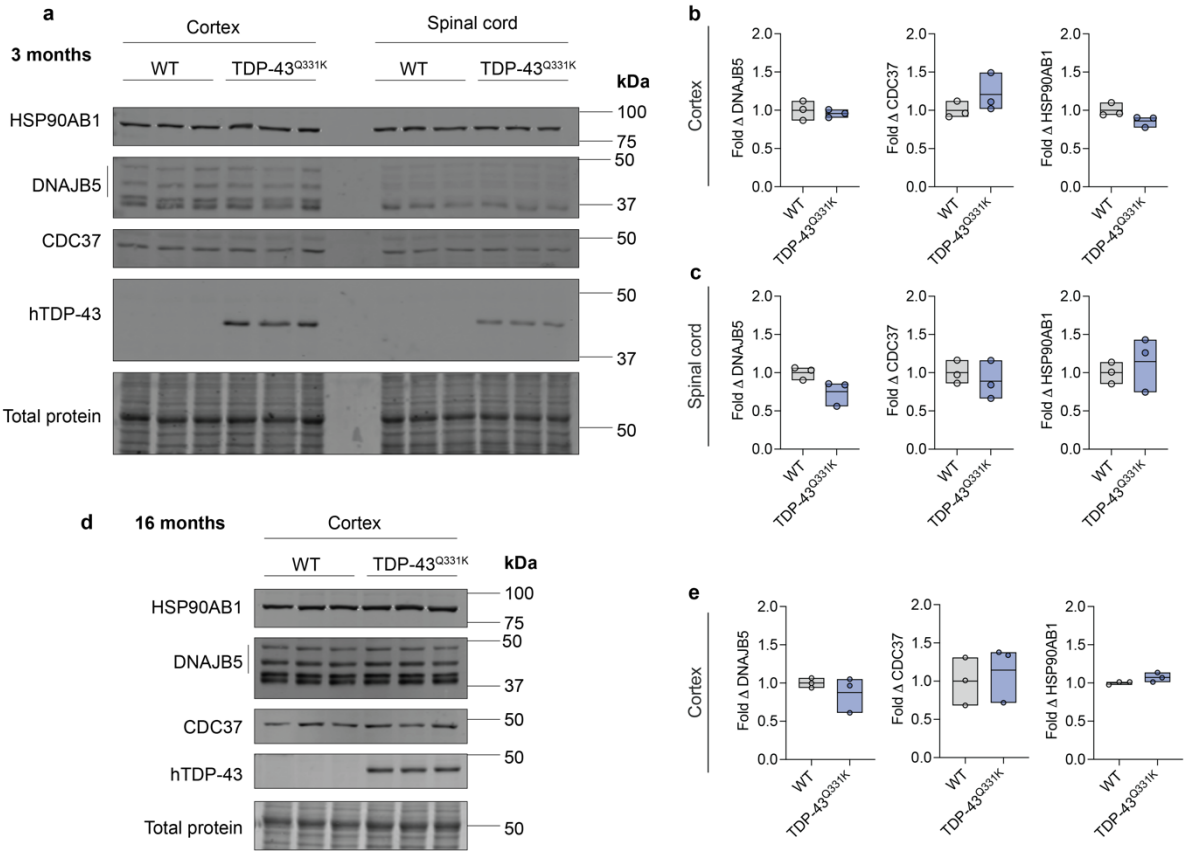


**Supplementary Figure 12. Magenta module chaperones are not altered in the cortex or spinal cord of TDP-43$^{Q331K}$ mice.** TDP-43$^{Q331K}$ and non-transgenic littermate controls were aged to 3 months, which represents a disease onset stage of the ALS model, or 16 months, a mid-disease stage. Cortex and spinal cord tissues were harvested for whole tissue homogenization and lysis in RIPA buffer. **a,** RIPA soluble protein lysates of cortex and spinal cord at 3 months, were immunoblotted and probed for magenta module chaperones HSP90AB1, DNAJB5, CDC37 and human TDP-43 (hTDP-43). **b,** Fold change of DNAJB5, CDC37, and HSP90AB1 in 3-month cortex tissue. **c,** Fold change of DNAJB5, CDC37, and HSP90AB1 in 3-month spinal cord tissue. **d,** RIPA soluble protein lysates of cortex from 16-month-old mice, were immunoblotted and probed for magenta module proteins HSP90AB1, DNAJB5, CDC37, and hTDP-43. **e,** Fold change of DNAJB5, CDC37, and HSP90AB1 in cortex at 16 months. Data are presented as open circles to represent individual mice (n = 3/group), and floating bars show the mean and range of the data. Differences between the means were determined using a paired t-test, where $P<0.05$ was considered statistically significant. Source data are provided as a Source Data file.

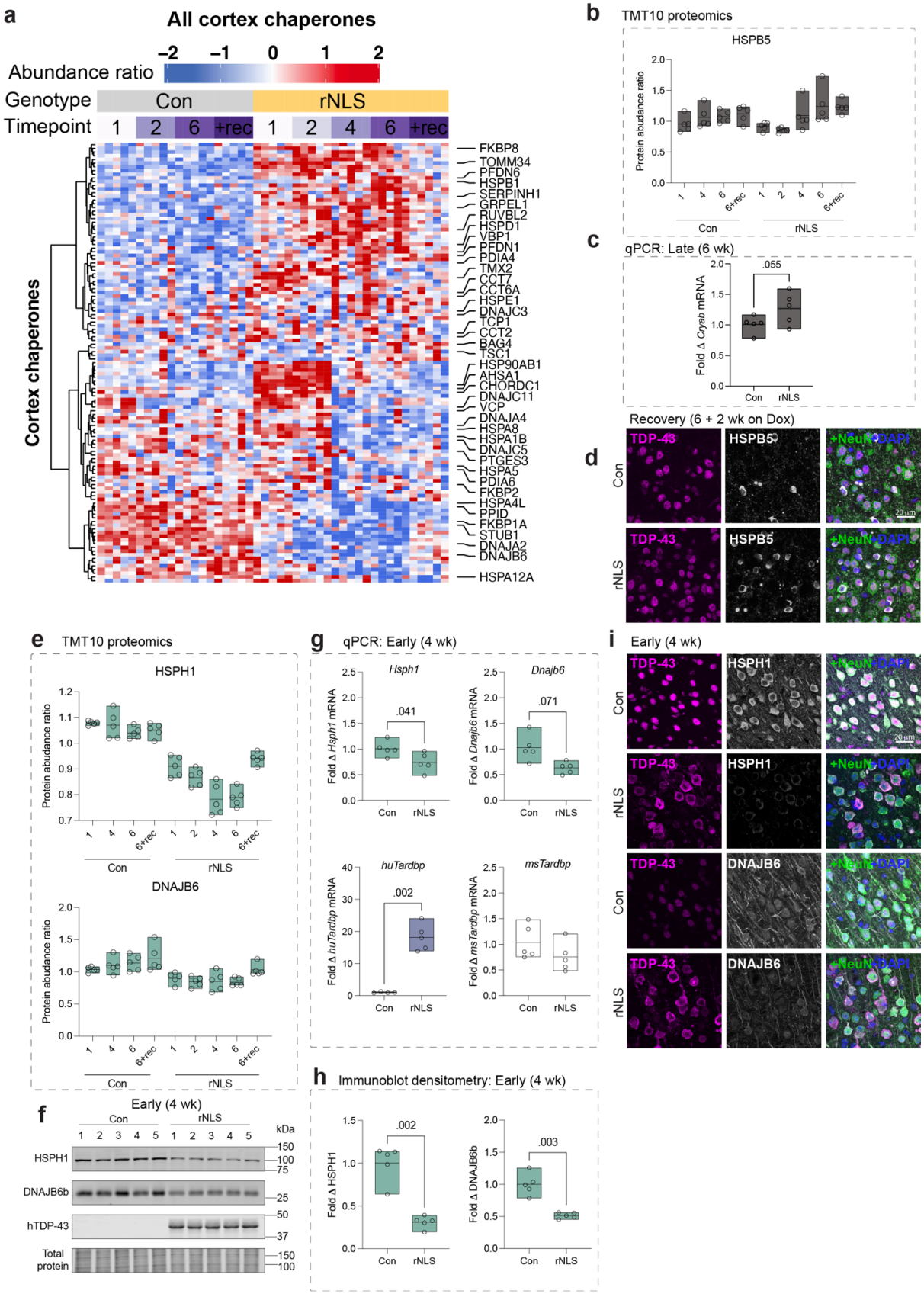


**Supplementary Figure 13. Chaperone proteins show diverging patterns of abundance in the rNLS8 cortex. a,** Heatmap of a subset of the longitudinal proteomics data representing 119 chaperones identified in the cortex. Samples are from control and rNLS8 mice 1, 2, 4, 6 weeks off dox and recovery mice (6 weeks off dox + 2 weeks on dox). Red is high and blue is low relative protein abundance. **b-d,**

Analysis of cortex tissue from recovery mice (6 wk off dox + 2 weeks on dox) **b,** Relative protein abundance of HSPB5 from quantitative longitudinal proteomics. **c,** Fold change in mRNA transcript level of *Cryab* (which codes for HSPB5) relative to the mean of control mice and normalized to the *Gapdh* housekeeping gene by qPCR. **d,** Immunofluorescence microscopy of the primary motor cortex in control and rNLS8 mice in recovery shows clearance of cytoplasmic TDP-43 and nuclear localization of TDP-43. Samples were immunolabeled for HSPB5, and co-labeled for TDP-43, NeuN (pan-neuronal marker), and DAPI. **e,** Protein abundance ratio from quantitative temporal proteomics of heat shock protein family H member 1 (HSPH1), and DnaJ heat shock protein family member (Hsp40) member B6 (DNAJB6). **f,** Immunoblot of RIPA-soluble whole cortex tissue lysates after 4 weeks of cytoplasmic TDP-43 expression. Tissue was probed for HSPH1 (105 kDa), DNAJB6b (26 kDa), and human TDP-43 (43 kDa). **h,** Immunoblot densitometry, fold change protein levels relative to the mean of control mice and normalized to total protein loading. **g,** Fold change in mRNA transcript level of target genes relative to the mean of control mice and normalized to the *Gapdh* housekeeping gene by qPCR. **i,** Immunofluorescence microscopy of the primary motor cortex in control and rNLS8 mice in early disease. Samples were immunolabeled for each target, HSPH1 and DNAJB6 (*top to bottom*), and co-labeled for TDP-43, NeuN (pan-neuronal marker), and DAPI. All data shown are from n = 5 mice per group (open circle points) with a line at the mean and range displayed by floating bars. Differences in the means of control and rNLS8 mice were determined using a two-tailed paired t-test, where a value of $P < 0.05$ was considered statistically significant. Scale bar = 20 μm. Source data are provided as a Source Data file.

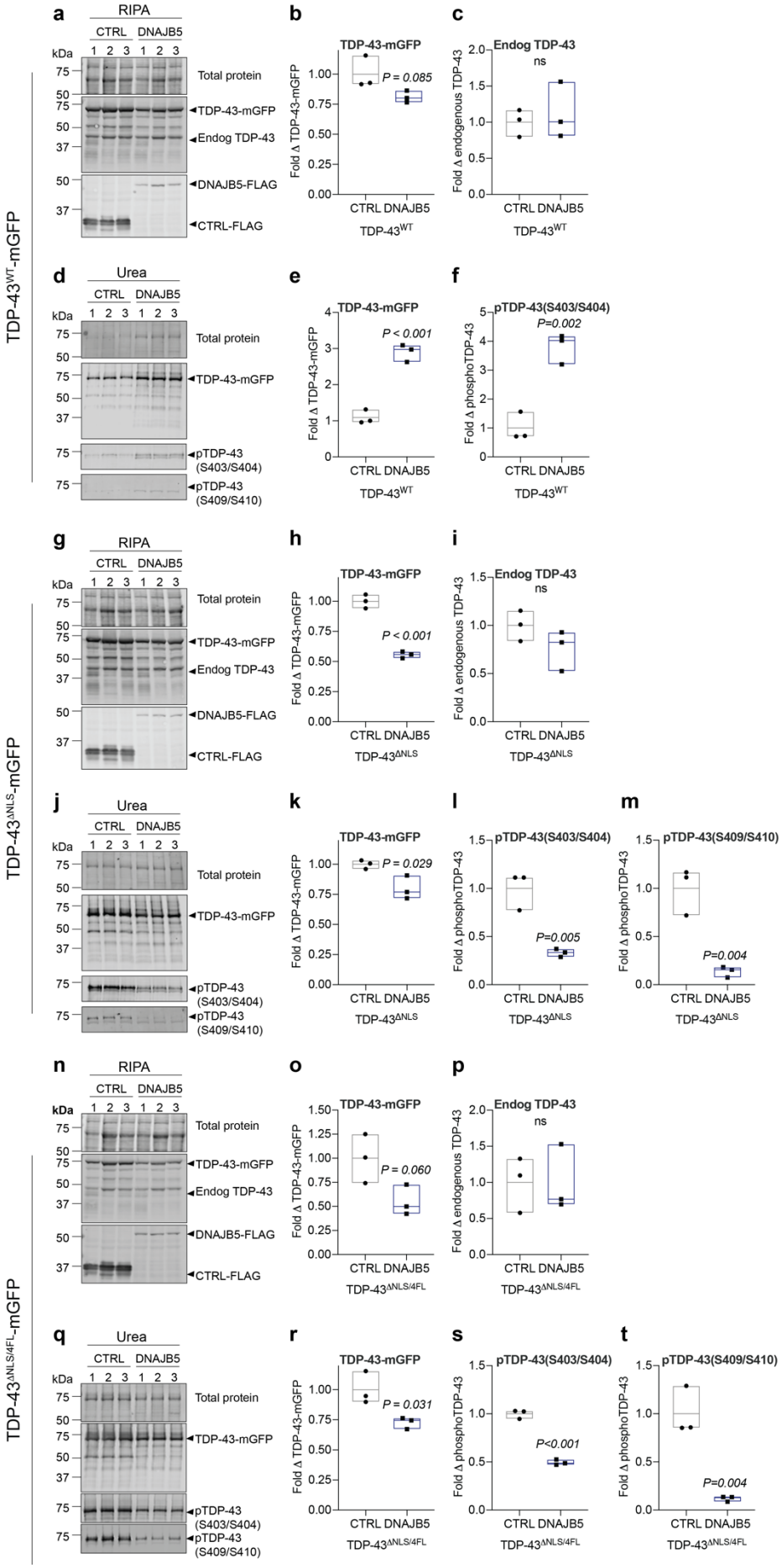
a
RIPA
CTRL DNAJB5
kDa
1 2 3 1 2 3
Total protein
TDP-43-mGFP
Endog TDP-43
DNAJB5-FLAG
CTRL-FLAG
b
TDP-43-mGFP
P = 0.085
Fold Δ TDP-43-mGFP
CTRL DNAJB5
TDP-43WT
c
Endog TDP-43
ns
Fold Δ endogenous TDP-43
CTRL DNAJB5
TDP-43WT
TDP-43WT-mGFP
d
Urea
CTRL DNAJB5
Total protein
TDP-43-mGFP
pTDP-43 (S403/S404)
pTDP-43 (S409/S410)
e
TDP-43-mGFP
P < 0.001
Fold Δ TDP-43-mGFP
CTRL DNAJB5
TDP-43WT
f
pTDP-43(S403/S404)
P=0.002
Fold Δ phosphoTDP-43
CTRL DNAJB5
TDP-43WT
g
RIPA
CTRL DNAJB5
Total protein
TDP-43-mGFP
Endog TDP-43
DNAJB5-FLAG
CTRL-FLAG
h
TDP-43-mGFP
P < 0.001
Fold Δ TDP-43-mGFP
CTRL DNAJB5
TDP-43ΔNLS
i
Endog TDP-43
ns
Fold Δ endogenous TDP-43
CTRL DNAJB5
TDP-43ΔNLS
TDP-43ΔNLS-mGFP
j
Urea
CTRL DNAJB5
Total protein
TDP-43-mGFP
pTDP-43 (S403/S404)
pTDP-43 (S409/S410)
k
TDP-43-mGFP
P = 0.029
Fold Δ TDP-43-mGFP
CTRL DNAJB5
TDP-43ΔNLS
l
pTDP-43(S403/S404)
P=0.005
Fold Δ phosphoTDP-43
CTRL DNAJB5
TDP-43ΔNLS
m
pTDP-43(S409/S410)
P=0.004
Fold Δ phosphoTDP-43
CTRL DNAJB5
TDP-43ΔNLS
n
RIPA
CTRL DNAJB5
Total protein
TDP-43-mGFP
Endog TDP-43
DNAJB5-FLAG
CTRL-FLAG
o
TDP-43-mGFP
P = 0.060
Fold Δ TDP-43-mGFP
CTRL DNAJB5
TDP-43ΔNLS/4FL
p
Endog TDP-43
ns
Fold Δ endogenous TDP-43
CTRL DNAJB5
TDP-43ΔNLS/4FL
TDP-43ΔNLS/4FL-mGFP
q
Urea
CTRL DNAJB5
Total protein
TDP-43-mGFP
pTDP-43 (S403/S404)
pTDP-43 (S409/S410)
r
TDP-43-mGFP
P = 0.031
Fold Δ TDP-43-mGFP
CTRL DNAJB5
TDP-43ΔNLS/4FL
s
pTDP-43(S403/S404)
P<0.001
Fold Δ phosphoTDP-43
CTRL DNAJB5
TDP-43ΔNLS/4FL
t
pTDP-43(S409/S410)
P=0.004
Fold Δ phosphoTDP-43
CTRL DNAJB5
TDP-43ΔNLS/4FL

**Supplementary Figure 14. Over-expression of DNAJB5 decreases soluble and insoluble mutant TDP-43 in HEK293 cells.** HEK293 cells were co-transfected to express wild-type or mutant forms of TDP-43-mGFP and DNAJB5-FLAG or a negative control (CTRL-FLAG). Cell lysates were fractionated into RIPA-soluble and urea-soluble fractions for immunoblotting. **a**, Immunoblot of RIPA-soluble TDP-$43^{WT}$-mGFP and densitometry of **b**, TDP-43, and **c**, endogenous TDP-43. **d**, Immunoblot of urea-soluble TDP-$43^{WT}$ and densitometry of **e**, TDP-$43^{WT}$-mGFP and **f**, phospho-TDP-43 (S403/S404). **g**, Immunoblot of RIPA-soluble TDP-$43^{\Delta NLS}$-mGFP and densitometry of **h**, TDP-$43^{\Delta NLS}$-mGFP, and **i**, endogenous TDP-43. **j**, Immunoblot of urea-soluble TDP-43 and densitometry of **k**, TDP-$43^{\Delta NLS}$-mGFP, **l**, phospho-TDP-43 (S403/S404), and **m**, phospho-TDP-43 (S409/S410). **n**, Immunoblot of RIPA-soluble TDP-43 and densitometry of **o**, TDP-$43^{\Delta NLS/4FL}$-mGFP, and **p**, endogenous TDP-43. **q**, Immunoblot of urea-soluble TDP-43 and densitometry of **r**, TDP-$43^{\Delta NLS/4FL}$-mGFP, **s**, phospho-TDP-43 (S403/S404), and **t**, phospho-TDP-43 (S409/S410). Statistically significant differences between the means were determined using unpaired t-tests, where $P < 0.05$ was considered significant. Data are from n = 3 independent experiments. Source data are provided as a Source Data file.

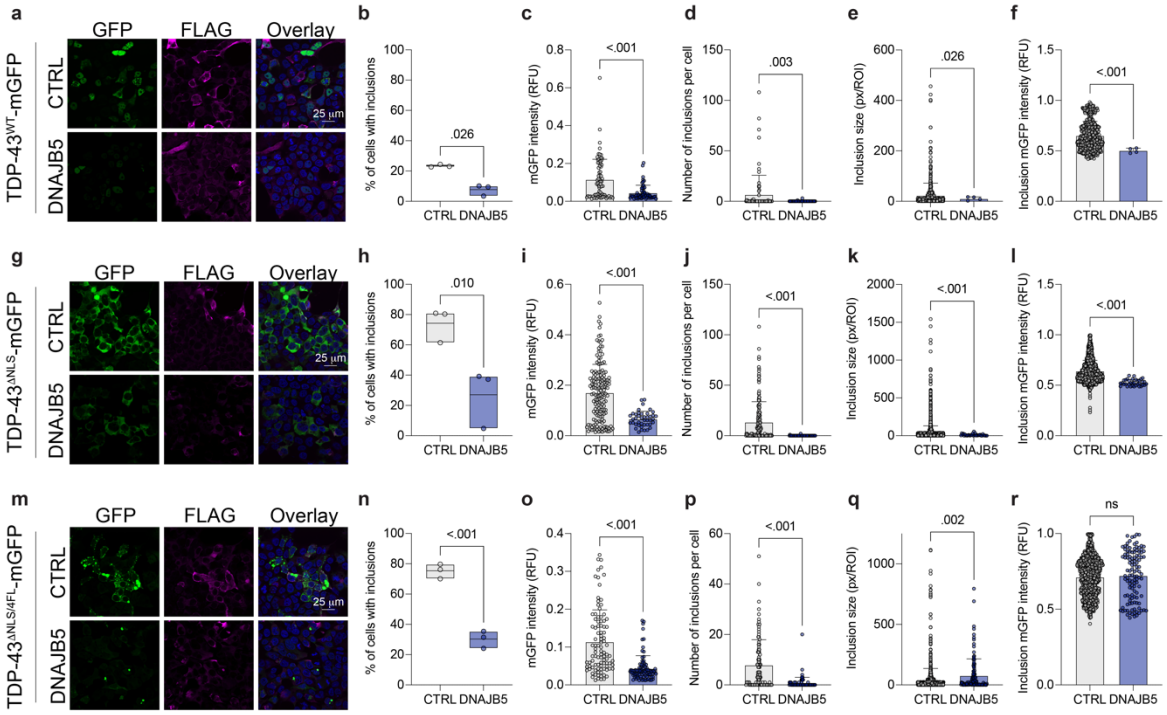


**Supplementary Figure 15. Over-expression of DNAJB5 decreases the proportion of cells with mutant TDP-43 inclusions and the number of inclusions per cell.** HEK293 cells were co-transfected to express wild-type or mutant forms of TDP-43-mGFP and DNAJB5-FLAG or a negative control (CTRL-FLAG). Cells were fixed and immunolabeled with anti-FLAG, imaged by microscopy, and subjected to non-biased single cell analysis using Cell Profiler. Cells over-expressing **a**, TDP-43$^{WT}$-mGFP, **g**, TDP-43$^{\Delta NLS}$-mGFP, or **m**, TDP-43$^{\Delta NLS/4FL}$-mGFP and CTRL or DNAJB5 were analyzed to determine **b/h/n**, the percent of cells with TDP-43WT-mGFP inclusions (data are from n = 3 independent experiments), **c/i/o**, fluorescence intensity of mGFP in relative fluorescence units (RFU), **d/j/p**, number of inclusions per cell, **e/k/q**, inclusion size, and **f/l/r**, inclusion mGFP fluorescence intensity. Statistically significant differences between the means were determined using unpaired Welch's t-tests, where $P < 0.05$ was considered significant. Single cell (c/i/o/d/j/p) and single inclusion (e/k/q/f/l/r) data are representative of n = 3 independent experiments. Source data are provided as a Source Data file.

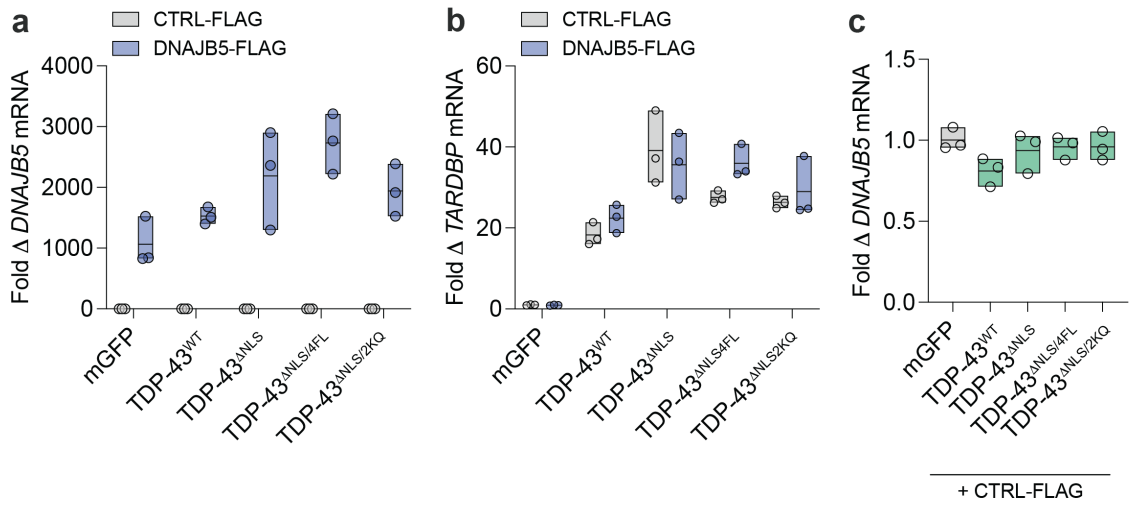


**Supplementary Figure 16. DNAJB5 overexpression does not alter exogenous TDP-43 transcription levels.** HEK293 cells were transfected to co-express wild-type or cytoplasmic mutant TDP-43 with DNAJB5-FLAG (or a negative control protein; CTRL-FLAG). Cells were lysed for RNA extraction, cDNA synthesis, and qPCR to quantify **a,** *DNAJB5* and **b,** *TARDBP* transcript levels. **c,** Fold change in endogenous *DNAJB5* transcripts in samples transfected with the negative control CTRL-FLAG plasmid (this data is replotted from **a**). Data is relative to the mean of the control sample (mGFP + CTRL-FLAG) and normalized to the *GAPDH* housekeeping gene. All data are from n = 3 independent experiments (open circles) with a line at the mean and the range displayed by floating bars. Differences in the means were determined using a one-way ANOVA and Dunnett's posthoc test, where $P < 0.05$ was considered statistically significant. Source data are provided as a Source Data file.

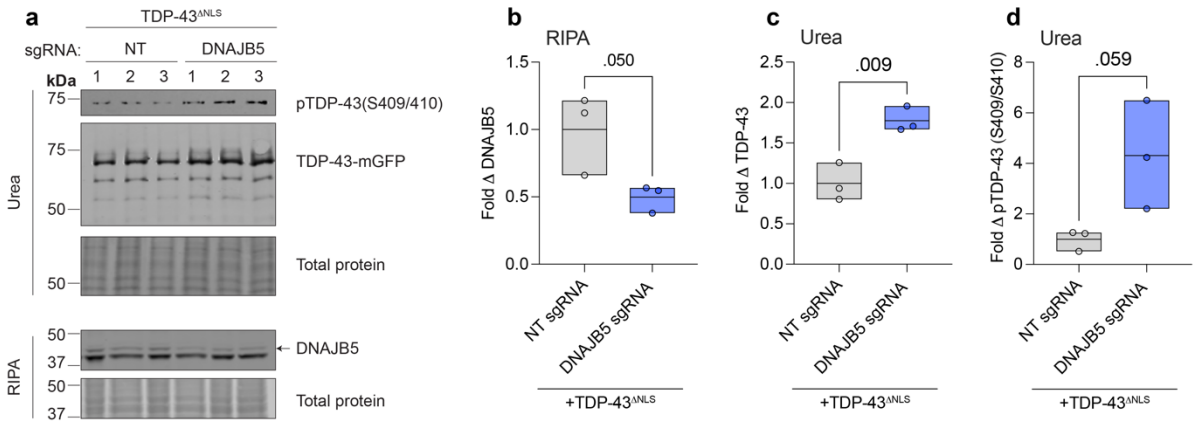


**Supplementary Figure 17. CRISPR knockout of DNAJB5 significantly increases insoluble TDP-43$^{\Delta NLS}$-mGFP levels.** HEK293 cells stably expressing Cas9 endonuclease, were co-transfected to express TDP-43$^{\Delta NLS}$-mGFP and sgRNA targeting *DNAJB5* or non-targeting (NT) negative control sgRNA. **a,** Cells were lysed and fractionated into soluble (RIPA) and insoluble (urea) protein fractions for immunoblot analysis of TDP-43 and DNAJB5 levels. **b,** Fold change insoluble DNAJB5 levels from immunoblot densitometry shows knockout of *DNAJB5*. **c,** Fold change insoluble TDP-43 levels. **d,** Fold change insoluble phosphoTDP-43 (S409/410) levels. All data are from n = 3 independent experiments (open circles) with a line at the mean and the range displayed by floating bars. Differences between the means were determined by a student's t-test and were statistically significant when $P < 0.05$. Source data are provided as a Source Data file.

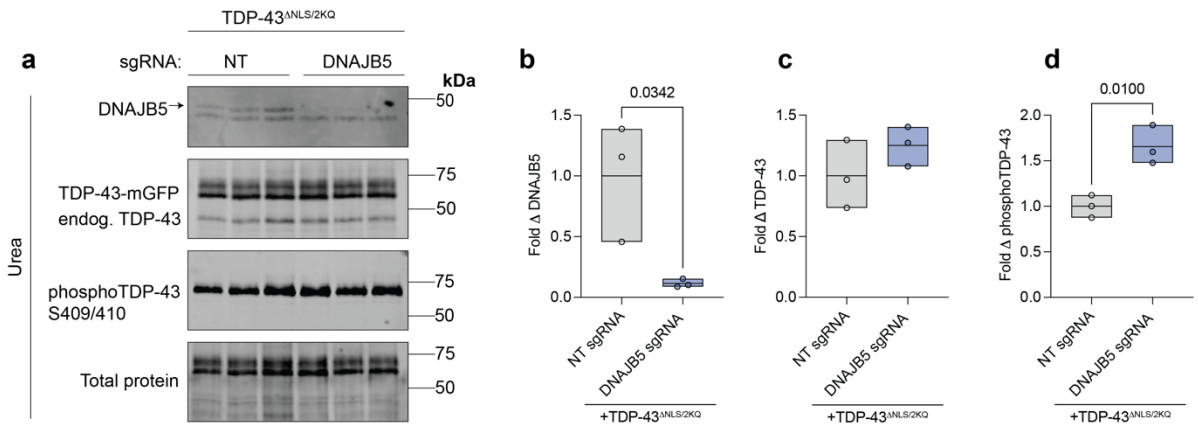


**Supplementary Figure 18. CRISPR knockout of DNAJB5 significantly increases insoluble cytoplasmic mutant TDP-43$^{\Delta NLS/2KQ}$-mGFP phosphoTDP-43 protein levels.** HEK293 cells stably expressing Cas9 endonuclease, were co-transfected to express TDP-43$^{\Delta NLS/2KQ}$ and sgRNA targeting *DNAJB5* or non-targeting (NT) negative control sgRNA. **a,** Cells were lysed and fractionated into insoluble (urea) protein fractions for immunoblot analysis of TDP-43 and DNAJB5 levels. **b,** Fold change insoluble DNAJB5 levels from immunoblot densitometry shows knockout of *DNAJB5*. **c,** Fold change insoluble TDP-43 levels. **d,** Fold change insoluble phosphoTDP-43 (S409/410) levels. All data are from n = 3 independent experiments (open circles) with a line at the mean and the range displayed by floating bars. Differences between the means were determined by a student's t-test and were statistically significant when $P < 0.05$. Source data are provided as a Source Data file.

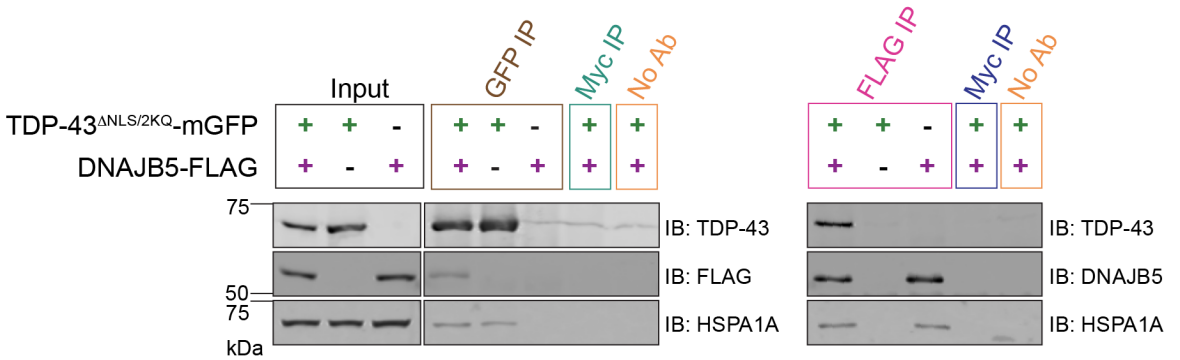


**Supplementary Figure 19. DNAJB5 interacts with soluble cytoplasmic TDP-43 to direct TDP-43 to HSPA1A for re-folding.** HEK-293 cells co-transfected or singly transfected to overexpress TDP-43$^{\Delta NLS/2KQ}$-mGFP and DNAJB5-FLAG were lysed in RIPA buffer to generate a soluble protein fraction. Immunoprecipitation (IP) experiments were conducted with rabbit anti-GFP (for pull-down of TDP-43$^{\Delta NLS/2KQ}$-mGFP) and mouse anti-FLAG (for pull-down of DNAJB5-FLAG). Technical controls were rabbit or mouse anti-Myc antibody and a no-antibody control to visualise non-specific interactions to beads. Input and immunoprecipitated samples were immunoblotted (IB) and probed for TDP-43, FLAG or DNAJB5 and HSPA1A. Data is representative of n = 3 independent experiments.

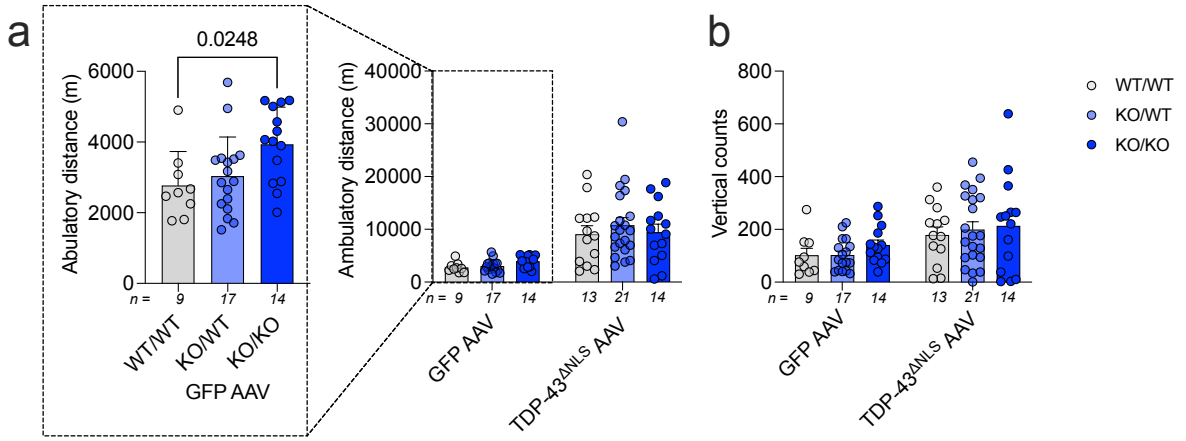


**Supplementary Figure 20. Open field behaviour testing of *Dnajb5* knockout mice injected with TDP-43$^{\Delta NLS}$-myc or GFP-myc (control) AAVs.** *Dnajb5* wildtype (WT/WT), heterozygous (KO/WT), and homozygous *Dnajb5* knockout (KO/KO) P0 pups were injected with human cytoplasmic TDP-43$^{\Delta NLS}$-myc or GFP-myc (control) AAVs via bilateral intracerebroventricular injections. Mice at 12 weeks of age were subjected to open field testing to assess their relative **a**, ambulatory distance (in meters) and **b,** vertical counts. Data shown is the mean + standard error of the mean and data points represent individual mice (*n* = 9-21/group, exact number of mice per group is noted in italics underneath each bar). Source data are provided as a Source Data file.

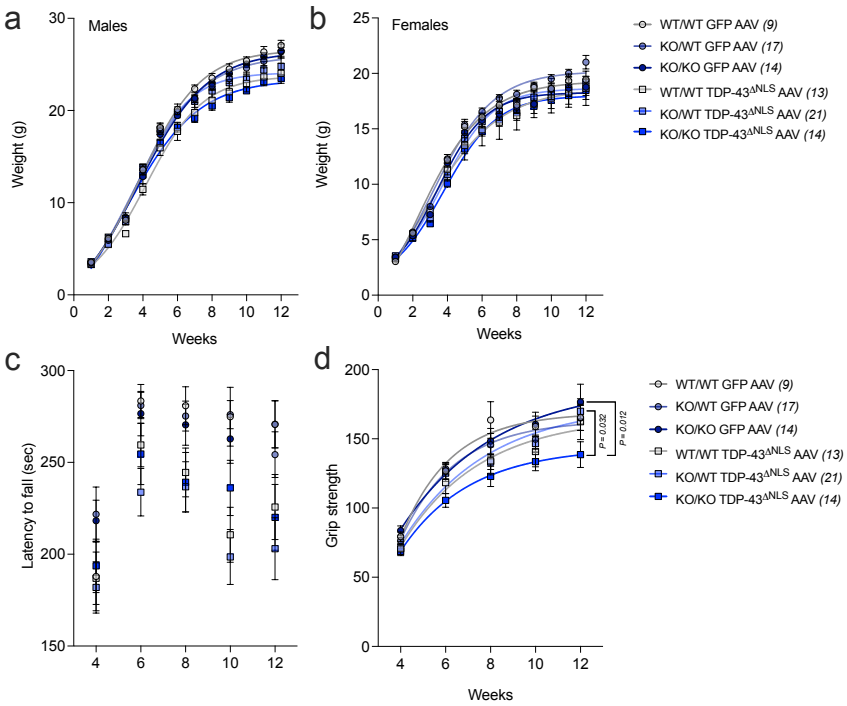


**Supplementary Figure 21. Weight and grip strength testing of *Dnajb5* knockout mice injected with TDP-43$^{\Delta NLS}$-myc or GFP-myc (control) AAVs.** *Dnajb5* wildtype (WT/WT), heterozygous (KO/WT), and homozygous *Dnajb5* knockout (KO/KO) P0 pups were injected with human cytoplasmic TDP-43$^{\Delta NLS}$-myc or GFP-myc (control) AAVs via bilateral intracerebroventricular injections. Mice were subjected to weekly weighing and grip strength testing every other week. **a**, Weight in grams of males over time. **b,** Weight in grams of females over time. **c,** Latency to fall in seconds in the rotarod test over time. **d**, Grip strength (gram force) of males and females combined over time. Data shown is the mean + standard error of the mean and data points represent individual mice (*n* = 9-21/group, exact number of mice per group is noted in italics in the key). Source data are provided as a Source Data file.

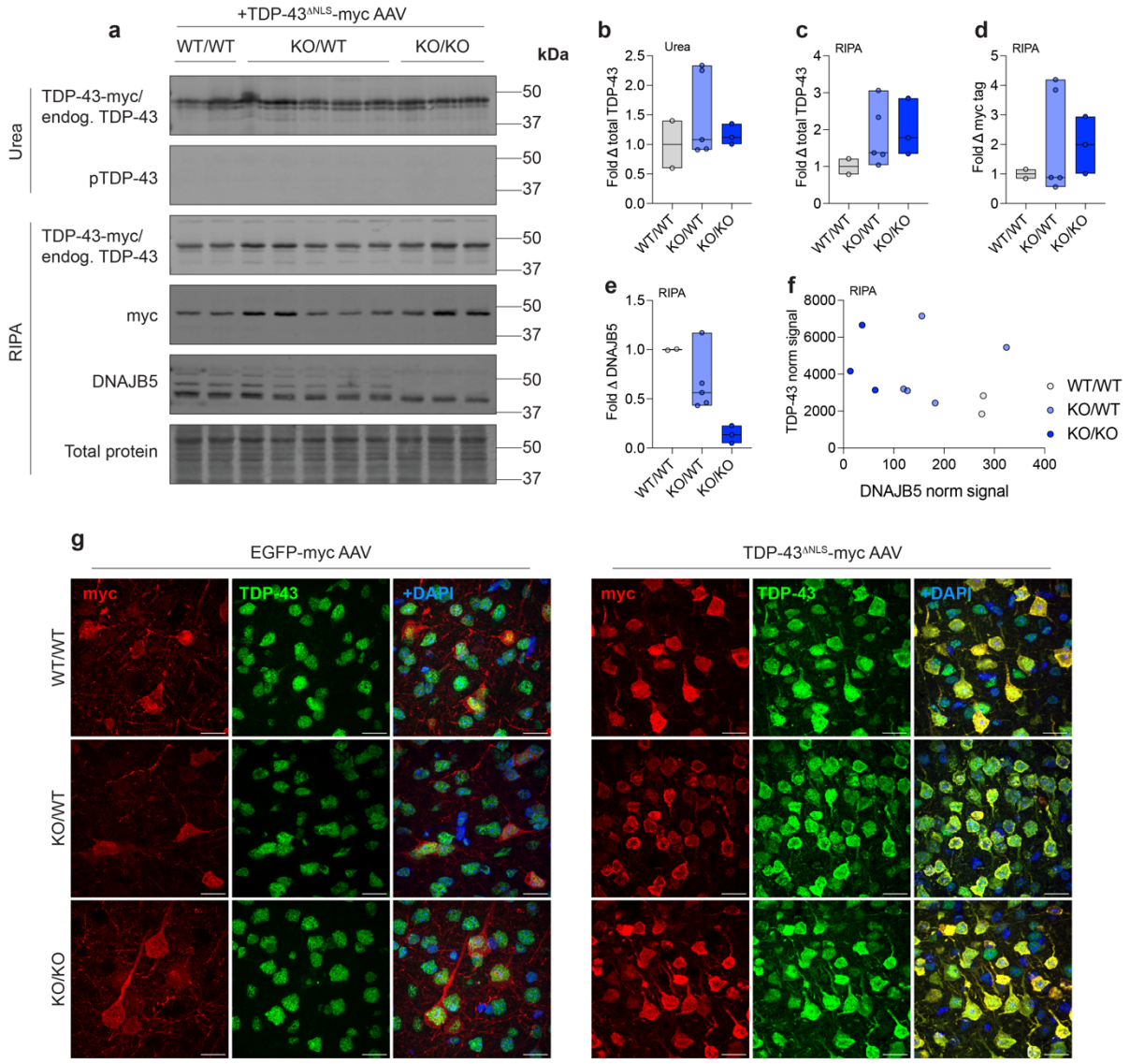


**Supplementary Figure 22. *Dnajb5* knockout does not exacerbate TDP-43 pathology after 3 months in mice injected with TDP-43$^{\Delta NLS}$-myc. a,** Immunoblot analysis of soluble and insoluble protein fractions from the cortex of 3 month old WT, heterozygous, and homozygous *Dnajb5* knockout mice injected with TDP-43$^{\Delta NLS}$-myc AAV. Immunoblots were probed for TDP-43, phosphoTDP-43, myc, and DNAJB5. **b,** Fold change in total insoluble TDP-43 levels. **c,** Fold change in total soluble TDP-43 levels. **d,** Fold change in myc-tagged TDP-43$^{\Delta NLS}$. **e,** Fold change in soluble DNAJB5 levels. **f,** Scatter plot showing relative TDP-43 levels as a function of DNAJB5 levels. **g,** Immunofluorescence microscopy of the cortex of 3-month-old WT, heterozygous, and homozygous *Dnajb5* knockout mice injected with EGFP-myc or TDP-43$^{\Delta NLS}$-myc AAV. Immunolabelled for myc, TDP-43, and nuclei counterstained with DAPI. Scale bar = 20 μm. Source data are provided as a Source Data file.

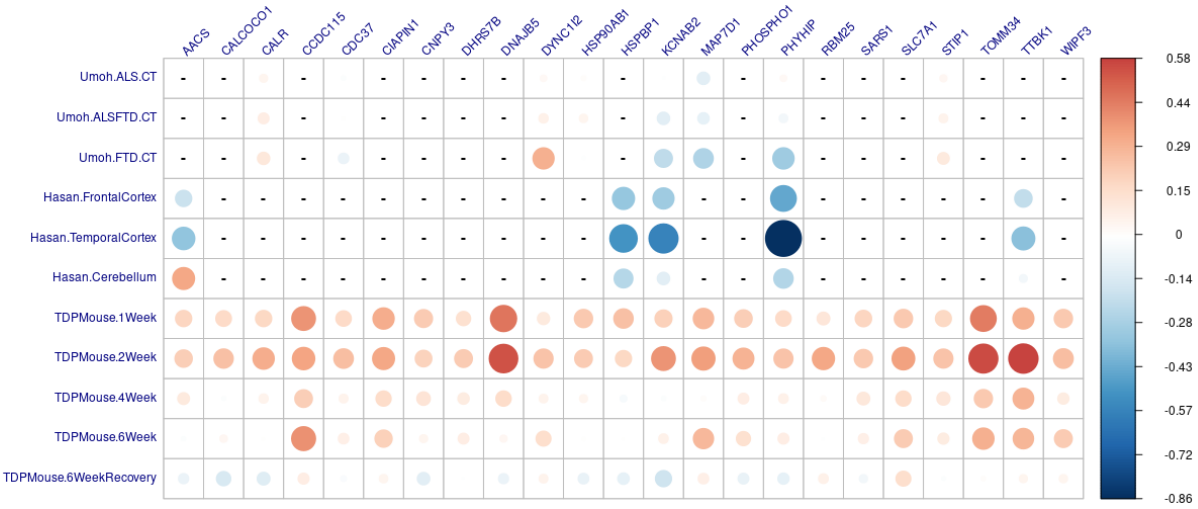


**Supplementary Figure 23. Protein/transcript abundance (log fold change) of protein folding magenta module proteins in human postmortem TDP-43 proteinopathies and the rNLS8 mouse cortex.** Proteins/transcripts for magenta module proteins are listed on the top and define each column. Each comparison made within each study is listed on the y-axis where each row of the table represents the log fold change of each protein/transcript in each comparison. Circle size is dependent on the magnitude of change and circle colour is dependent on log fold change where blue is decreased and red is increased compared to controls. Source data are provided as a Source Data file.

**Uncropped blots**

Related to Supplementary Figure 5 d

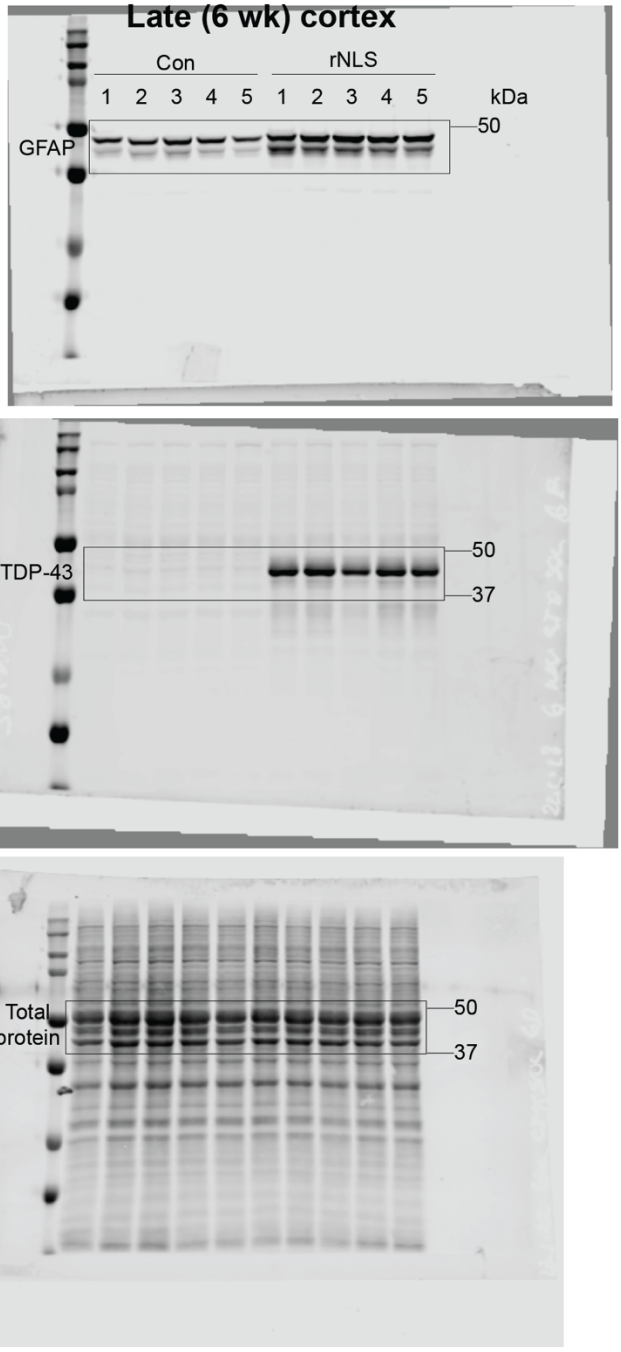

Related Supplementary Figure 6 d

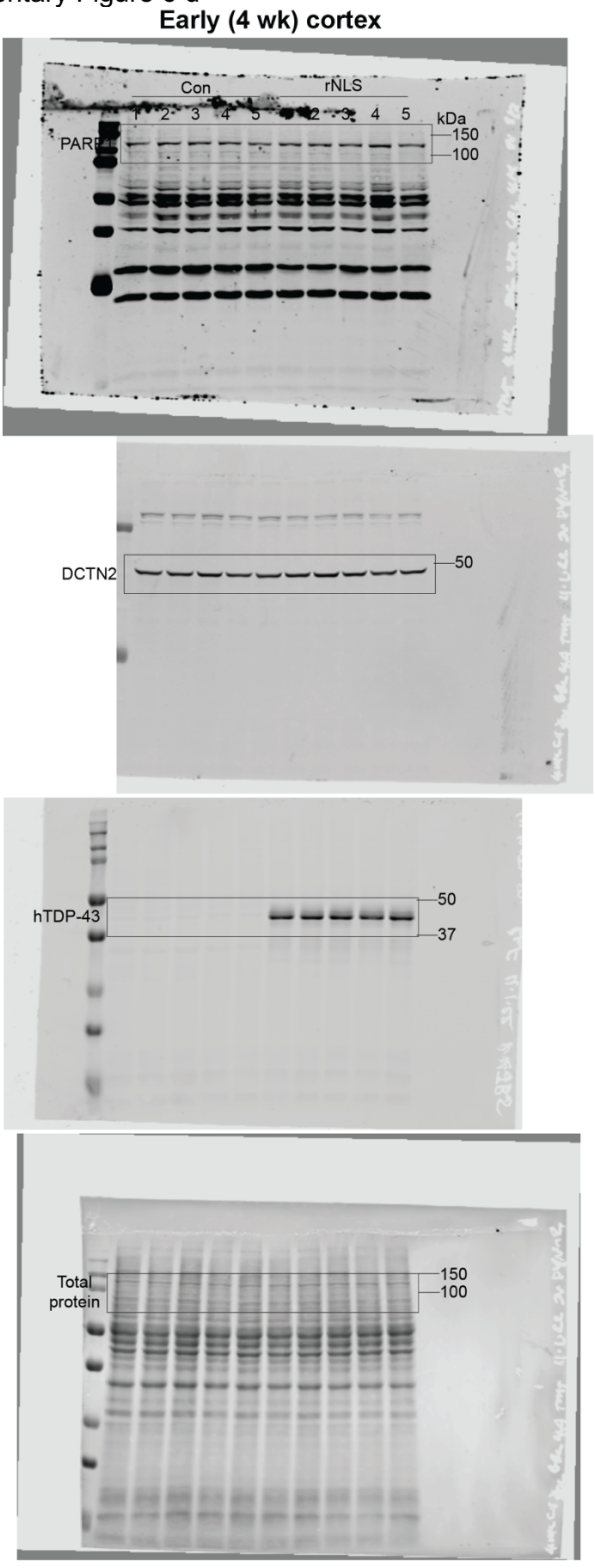

Related to Supplementary Figure 7

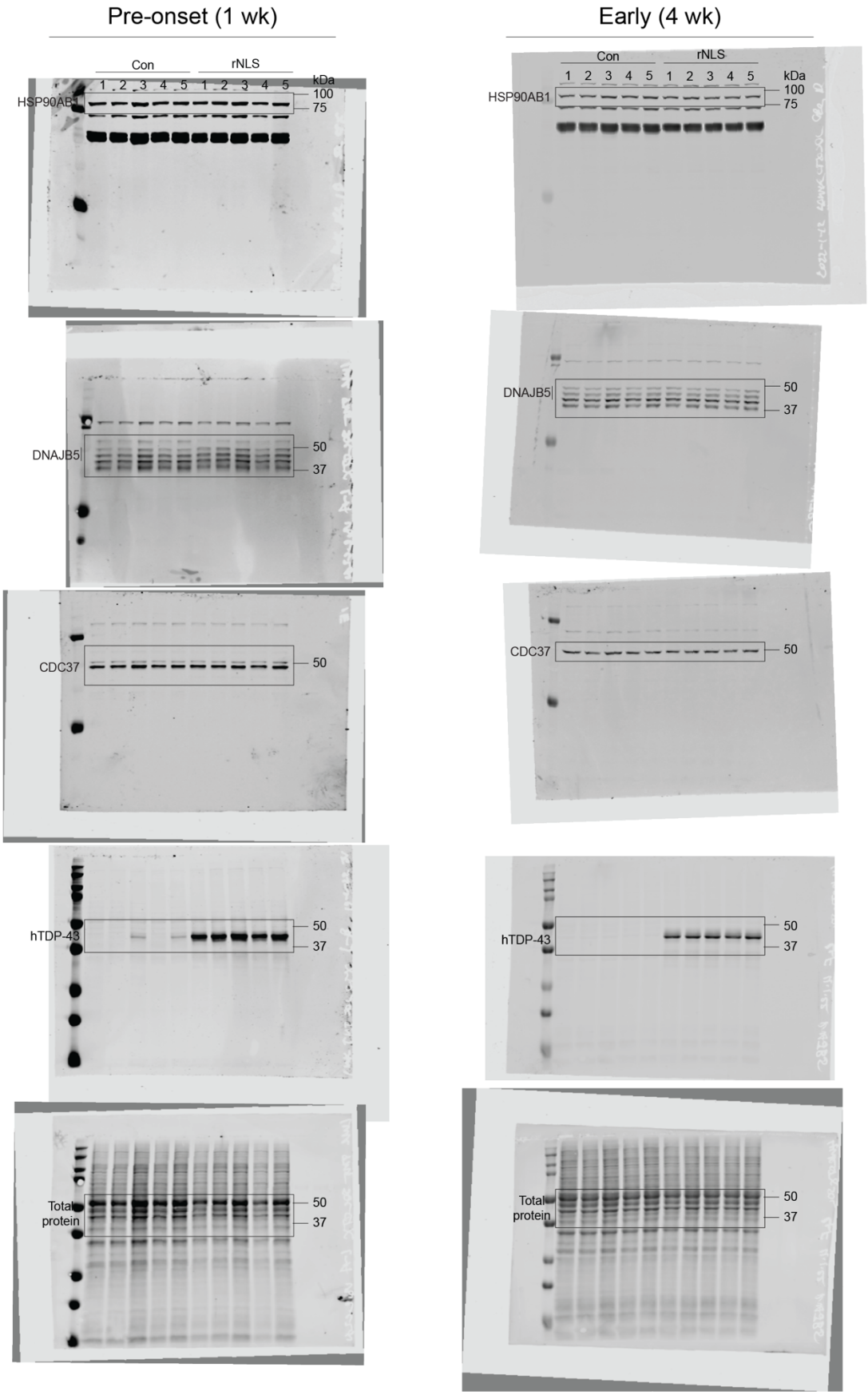

Related to Supplementary Figure 8

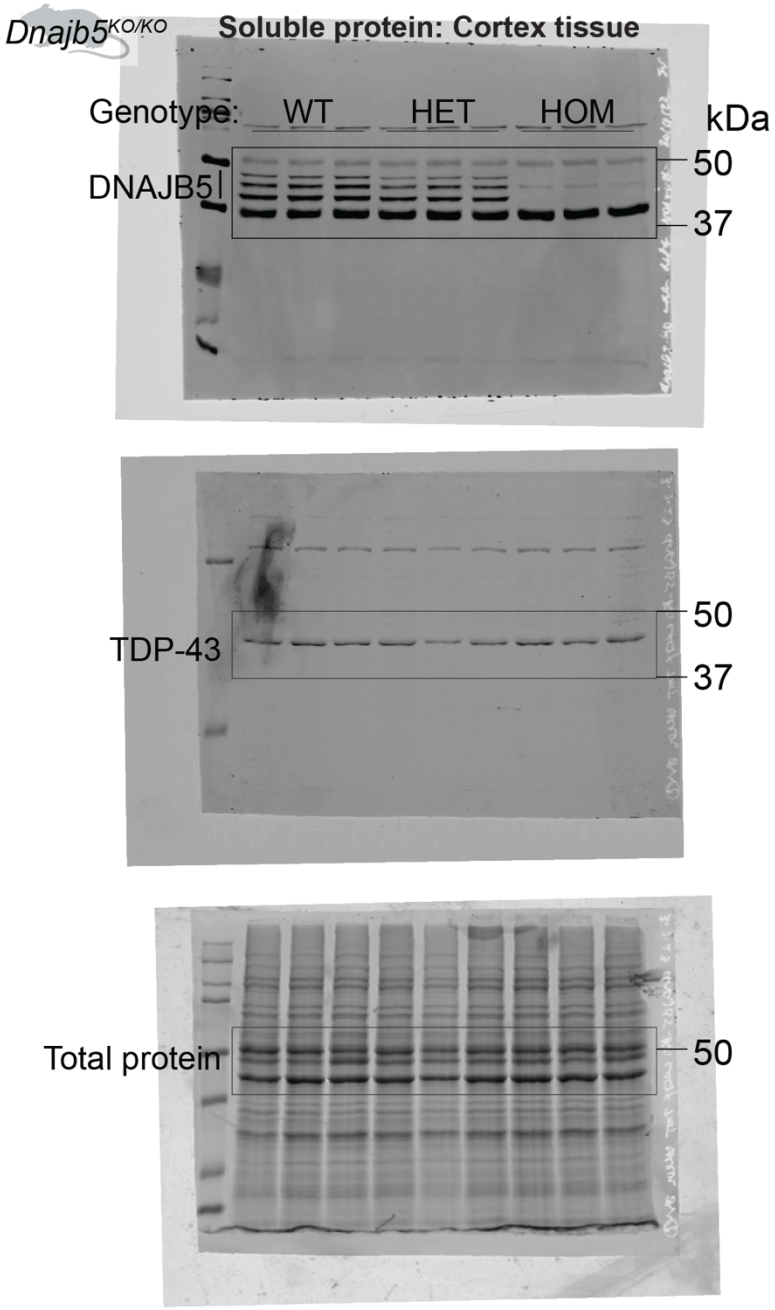

Related to Supplementary Figure 9

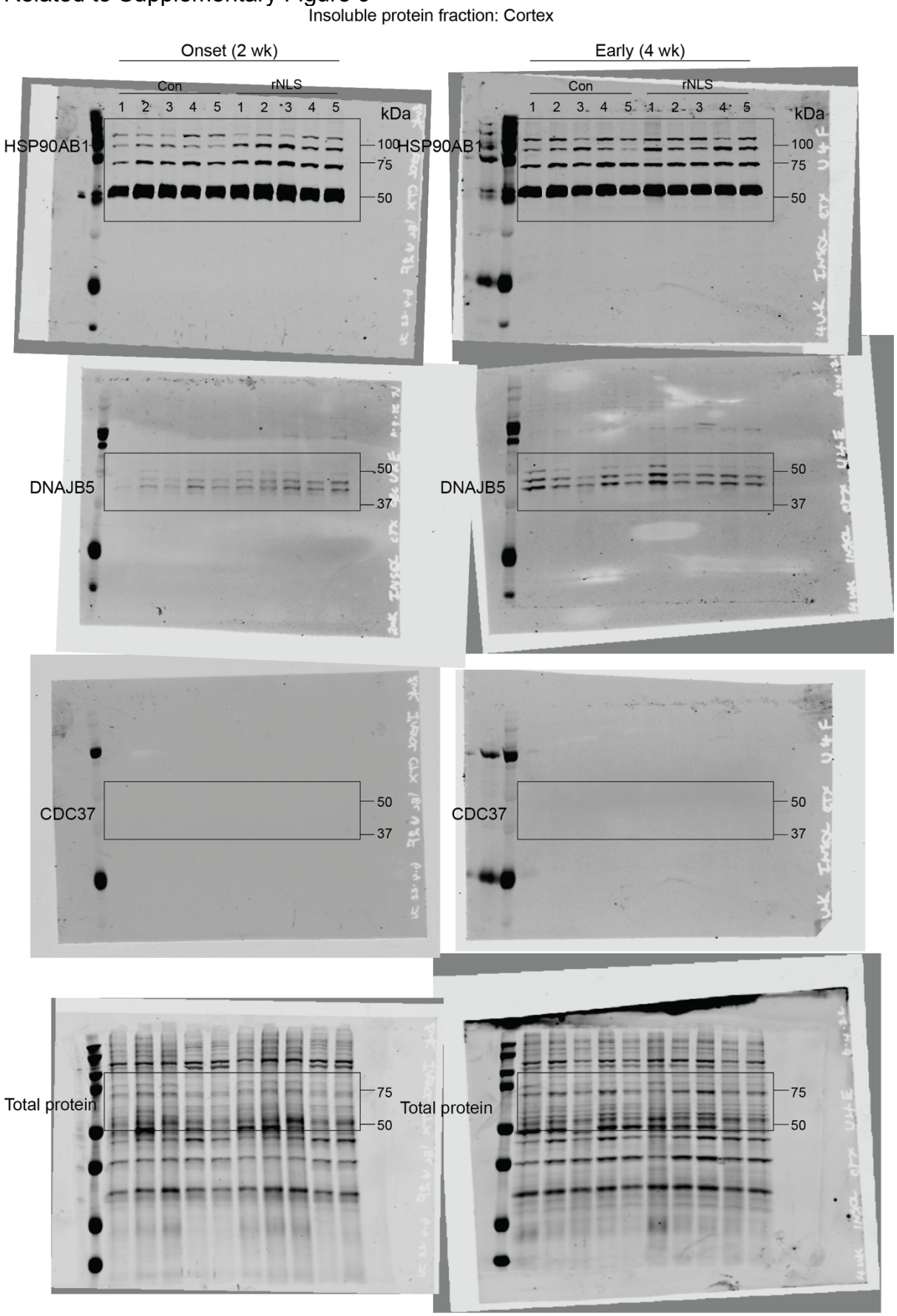

Related to Supplementary Figure 11

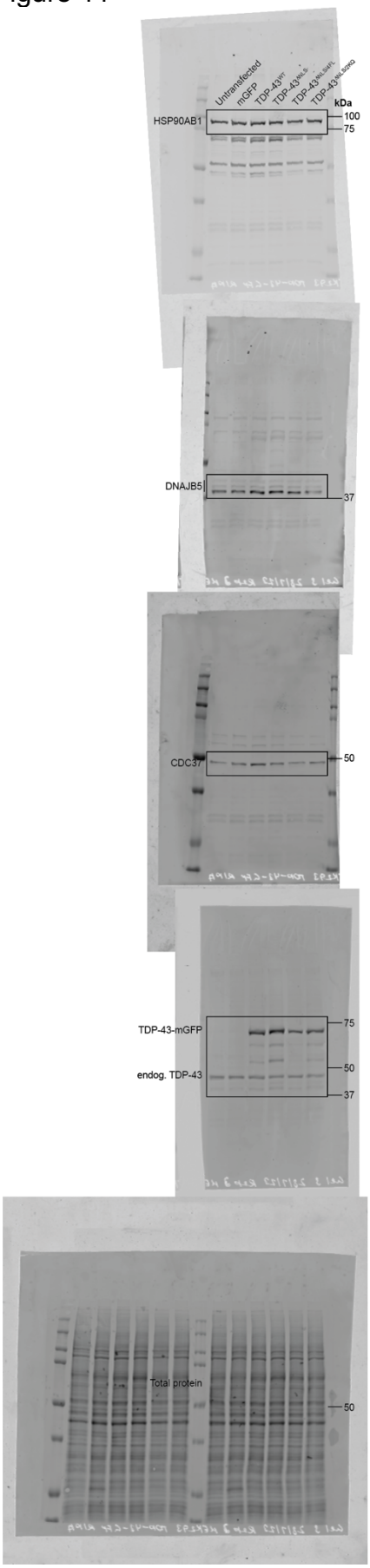

Related to Supplementary Figure 12

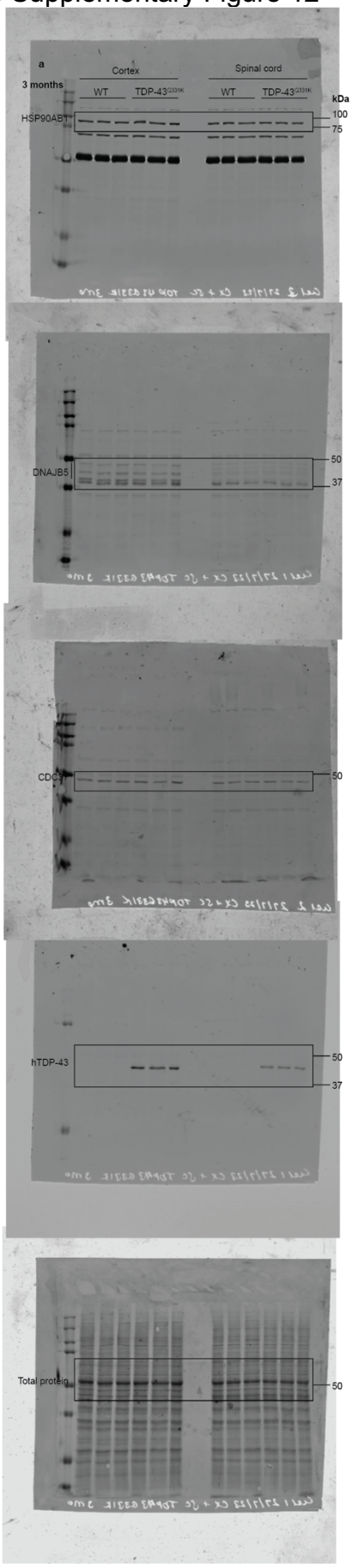


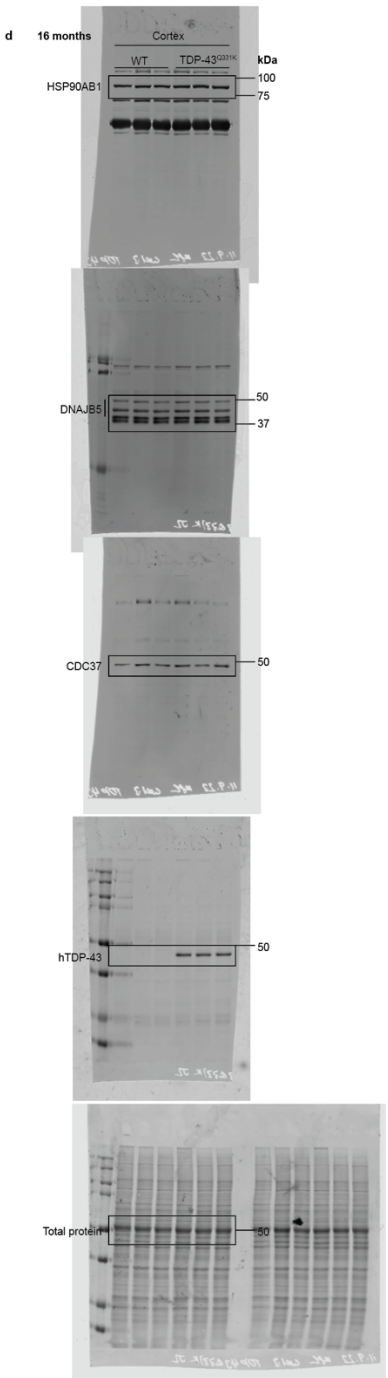

Related to Supplementary Figure 13 f

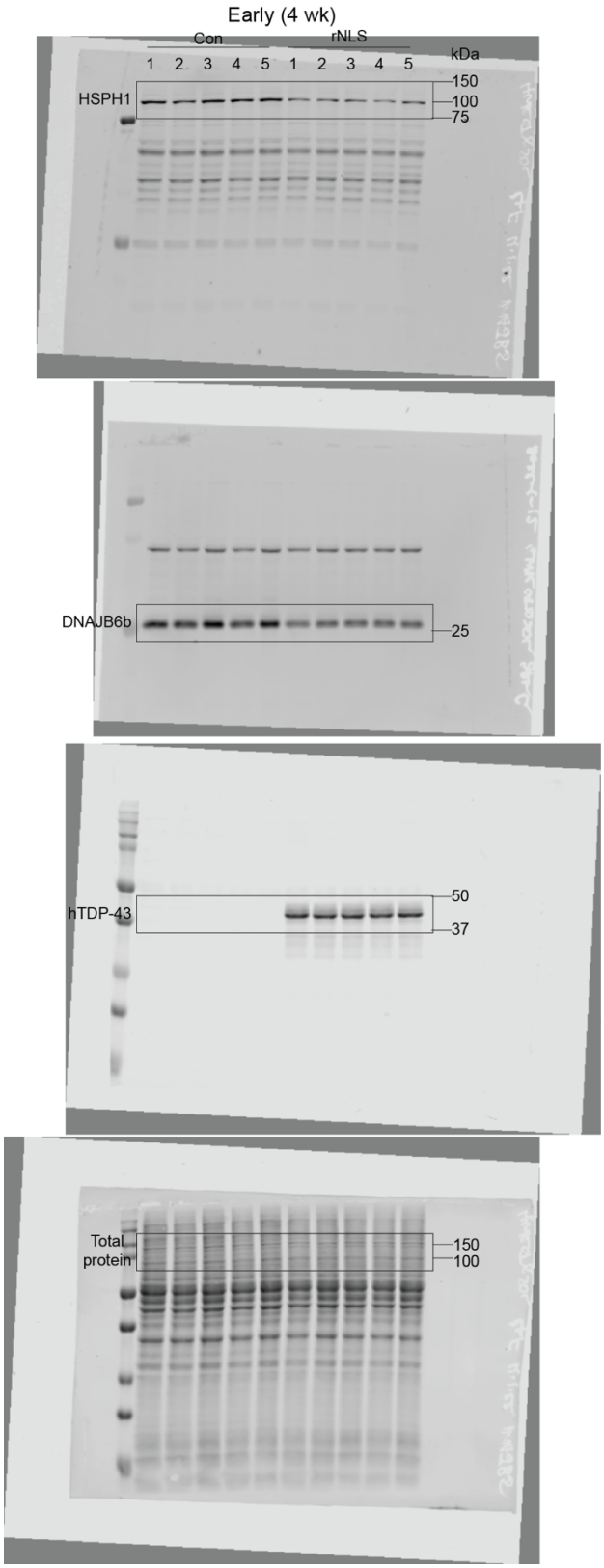

Related to Supplementary Figure 14

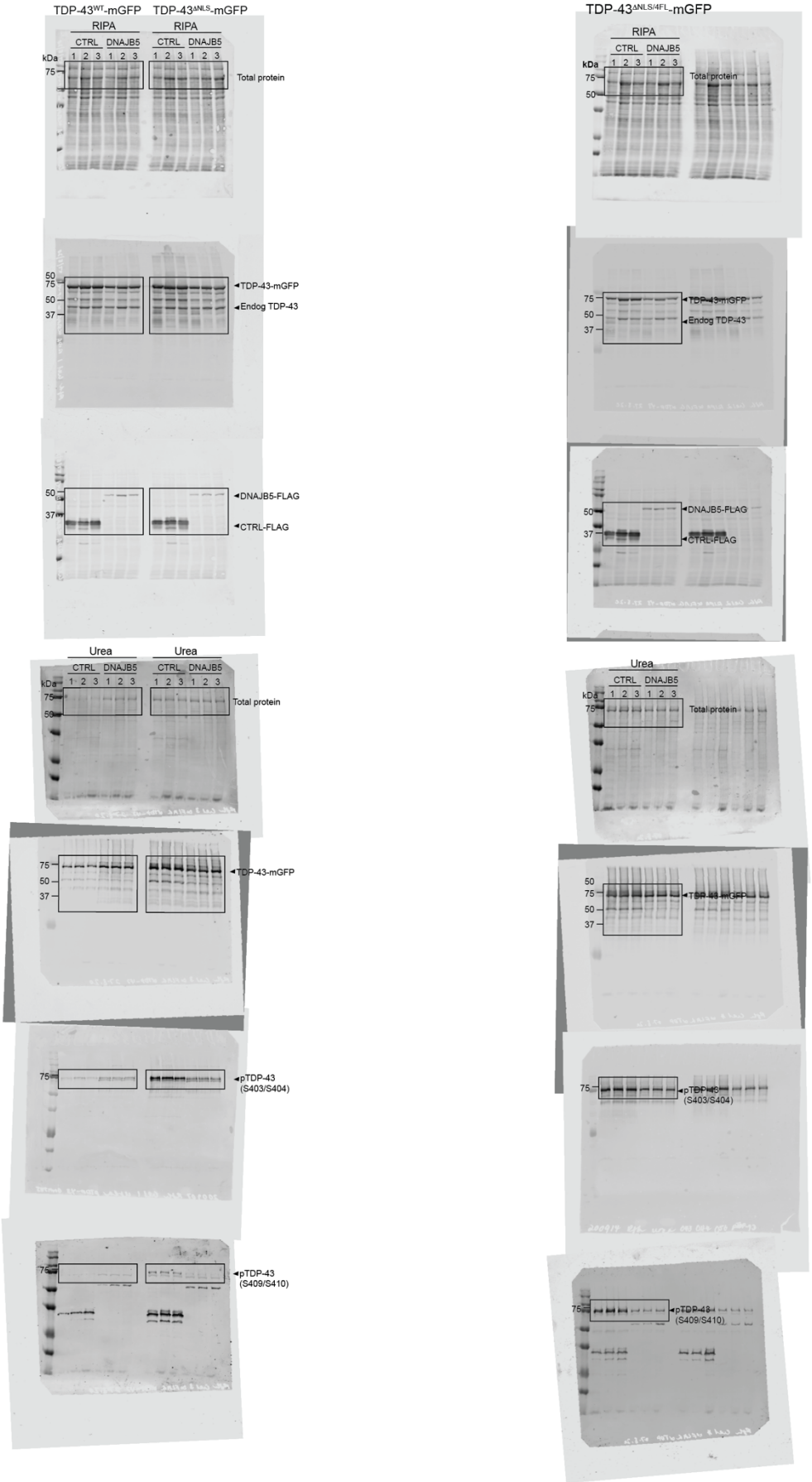

Related to Supplementary Figure 17 a

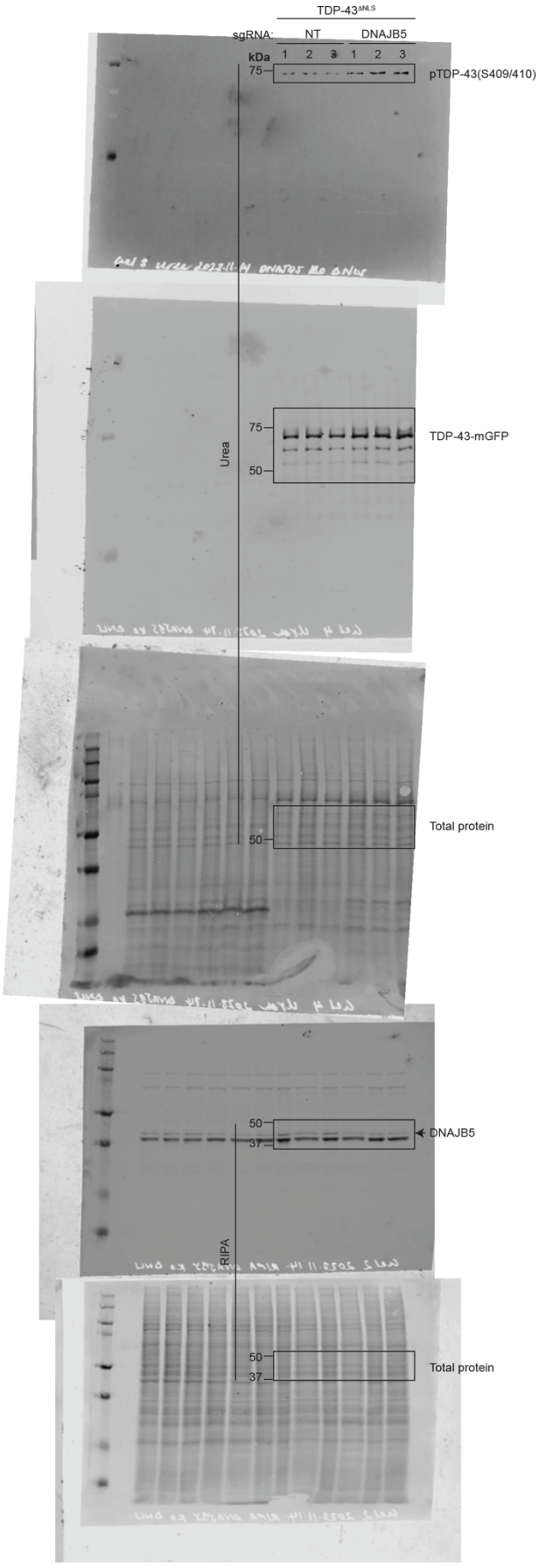

Related to Supplementary Figure 18

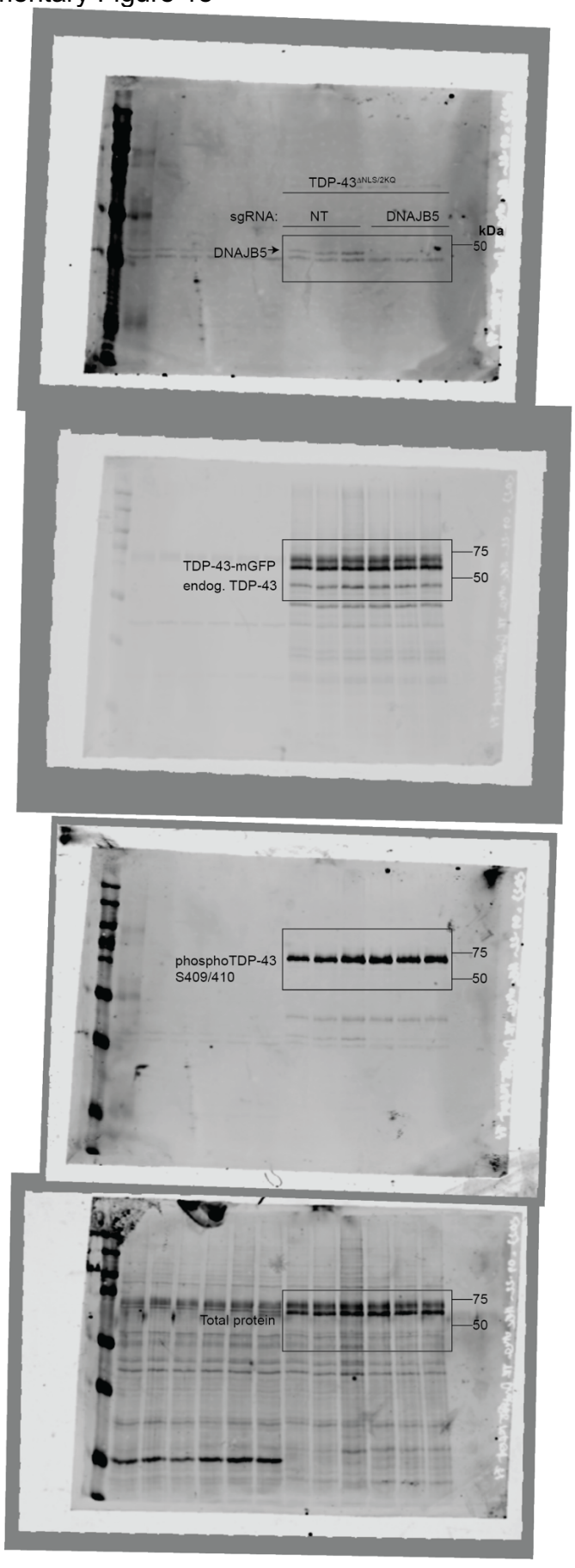

Related to Supplementary Figure 19

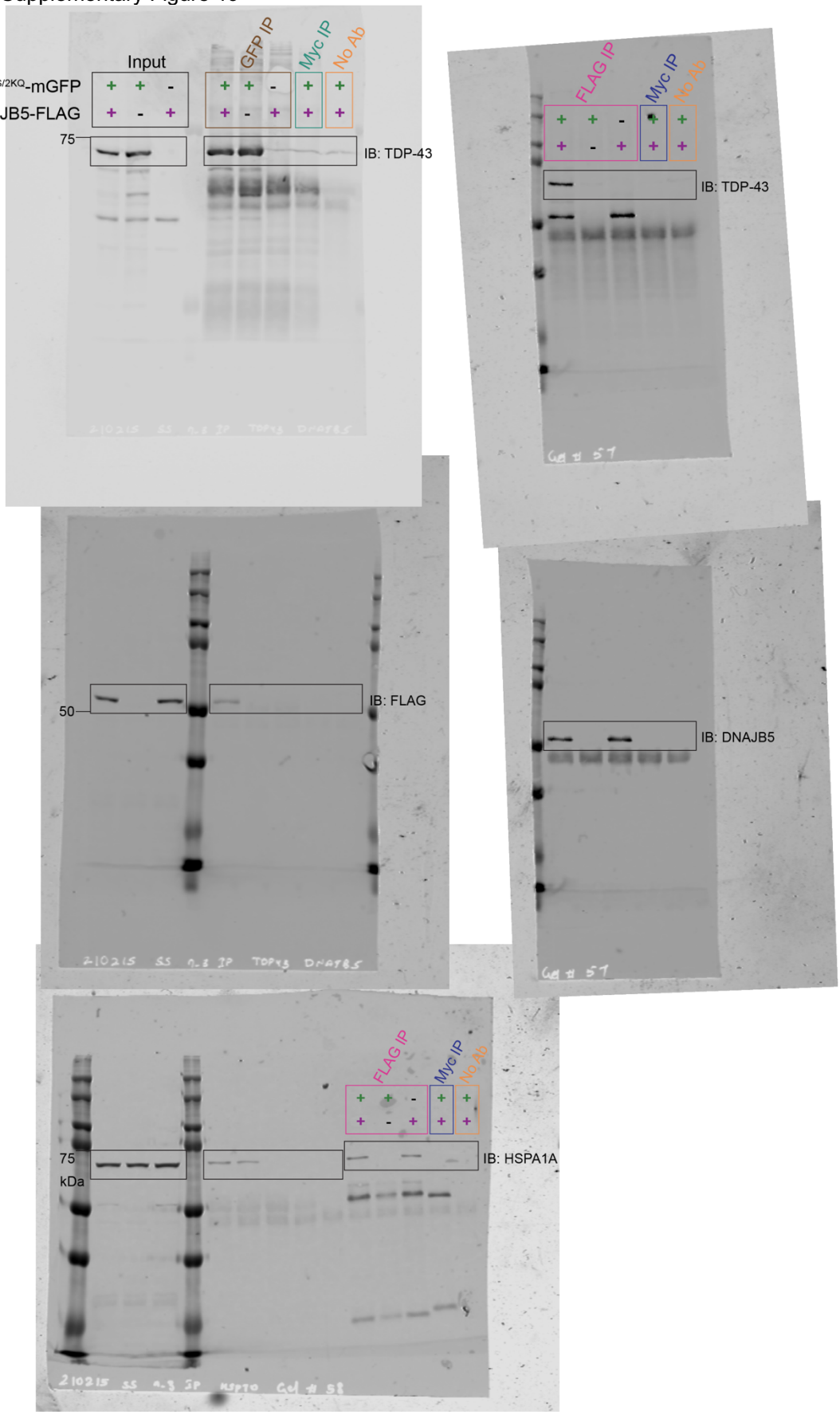

Related to Supplementary Figure 22 a